Temperature drives transcriptomic shifts in amphibian skin bacterial communities with consequences for fungal pathogen control

Running title: Temperature affects amphibian microbiome

Authors: Emma G. Thompson[1] & Elle M. Barnes[1]*

[1] Thomas H. Gosnell School of Life Sciences, Rochester Institute of Technology, New York, USA

* Corresponding Author: Elle M. Barnes; mailing address: 84 Lomb Memorial Dr, Rochester NY, USA 14623, email: embsbi@rit.edu

Keywords: *Batrachochytrium dendrobatidis*, *Batrachochytrium salamandrivorans*, amphibian microbiome, temperature-mediated effects, chytrid fungus, metatranscriptomics

Abstract

The chytrid fungi *Batrachochytrium dendrobatidis* (Bd) and *Batrachochytrium salamandrivorans* (Bsal) are two of the largest threats to amphibian populations worldwide. While the amphibian skin microbiome can inhibit these fungal pathogens, microbial composition varies substantially across host and environmental contexts. In addition, habitat-wide mitigation methods that capitalize on the thermal mismatch between Bd/Bsal and their hosts (e.g., warming the host or environment) have been proposed to combat infection. Preliminary experimental application of these methods shows promising results for host infection load, but has yet to consider the indirect effects that warming has on the microbiome. Here, we exposed synthetic microbial communities–comprising ten core members of the blue-spotted salamander (*Ambystoma laterale*) skin microbiome–and Bd/Bsal to five different temperatures reflecting proposed mitigation methods and a climate change scenario. Microbial community composition and gene expression were assessed via metabarcoding and metatranscriptomics. We found that both temperature and time play a significant role in shaping community composition. Temperature exerted a small but significant effect on Bd/Bsal inhibition, indicating that microbe-mediated mechanisms likely act alongside host physiological responses during thermal shifts. Metatranscriptomic profiling revealed distinct differential expression of bacterial genes involved in secretion systems, antimicrobial compound resistance, and heat-shock across temperature treatments. These findings demonstrate that thermal mitigation strategies can alter both microbiome composition and function, highlighting the need to account for off-target microbial responses when designing environmental disease interventions.

Introduction

Amphibians are essential and diverse components of global terrestrial and aquatic ecosystems, consisting of over 9,000 species [1,2]. However, an estimated 41% of amphibian species are threatened with extinction, driven by habitat loss, climate change, and emerging infectious diseases [2]. Among these threats, the panzootic chytrid fungi *Batrachochytrium dendrobatidis* (Bd) and its sister species *Batrachochytrium salamandrivorans* (Bsal; the causative agents of chytridiomycosis) represent unprecedented declines in amphibian biodiversity [3]. While Bd has impacted global amphibian populations for decades, Bsal selectively infects urodeles (salamanders and newts), triggering severe die-offs across Europe [3]. The potential introduction of Bsal to North America–the world's primary hotspot for salamander diversity–poses an imminent threat, as current biosecurity measures and trade restrictions are unlikely to completely prevent pathogen entry [4,5].

To combat chytridiomycosis, amphibians rely on innate physiological defenses (e.g., skin sloughing and antimicrobial peptides), behavioural thermoregulation, and a complex skin microbiome [4,6]. The skin microbiome functions as an extension of the host immune system wherein commensal microorganisms inhibit Bd and Bsal directly through the secretion of antifungal metabolites and indirectly through nutrient and niche competition (**Figure 1A**) [4,6–12]. However, host-microbiome-pathogen dynamics are highly sensitive to environmental context. Abiotic shifts, particularly temperature fluctuations, modulate host immune function and alter microbial community structure [13,14]. Despite growing recognition of these interactions, how thermal shifts directly alter the functional and transcriptomic output of the microbiome remains poorly understood.

The thermal optima of chytrid fungi, amphibian hosts, and cutaneous bacteria often diverge. Bd grows optimally between 17-24°C [10], whereas Bsal is adapted to cooler temperatures (10-15 °C) [3,11,12]. In contrast, many skin-associated bacteria and amphibian hosts exhibit broader thermal tolerances [15]. This thermal mismatch has inspired habitat-wide disease mitigation strategies designed to artificially elevate environmental temperatures–such as environmental pond warming or constructing heated microhabitats ("thermal hotspots")–to suppress fungal growth and alleviate host infection load [4,12,16,17]. Furthermore, climate change is independently altering environmental temperatures across amphibian ranges.

While thermal interventions hold promise for pathogen suppression, their consequences on the protective skin microbiome have yet to be sufficiently evaluated. Warming may alter bacterial composition or disrupt the expression of key functions responsible for antifungal defense (**Figure 1B**). To resolve these indirect effects without the confounding influence of host physiological responses, we leveraged a synthetic microbial community (SynCom) composed of ten core bacterial isolates from the skin of blue-spotted salamanders (*Ambystoma laterale*). We exposed this SynCom (co-cultured with Bd or Bsal) to five temperature regimes reflecting proposed thermal mitigation strategies and climate change predictions. Using integrated metabarcoding and metatranscriptomics, we tested the hypothesis that elevated temperatures disrupt microbial community structure and downregulate functional genes associated with antimicrobial production and stress responses, ultimately altering the microbiome's capacity for pathogen inhibition.

Methods

Culture Acquisition

In Fall 2023, we collected swabs from the skin of the salamander species *Ambystoma laterale* (n = 10) from the forested wetlands of the Rochester Institute of Technology in Rochester, NY, USA. Rochester's temperate climate and warming winter temperatures make the study site ideal for observing the impact of environmental warming on an abundant, cold-adapted salamander [18]. Swabs were immediately struck onto R2A agar and grown at 23°C until growth was evident. Morphologically distinct colonies were then isolated to pure cultures and extracted using the Prepman Ultra Sample Preparation Reagent (Thermo Fisher Scientific). The full-length 16S rRNA gene was amplified using the 27F (5'-AGAGTTTGATCCTGGCTCAG-3') and 1492R (5' -TACCTTGTTACGACTT- 3') primer pair [19] on a SimpliAmp thermal cycler (Thermo Fisher Scientific) in 25 µL reactions consisting of: 12.5 µl of 2X GoTaq Master Mix (Promega), 1 µl each of 10 µM forward and reverse primers, and 2 µl of DNA (~50 ng/µL). Samples were amplified with the following parameters: 95°C for 2 min, 30 cycles of 95°C for 30 seconds, 55°C for 30 seconds, and 72°C for 1 minute and 40 seconds, then 72°C for 10 min. The PCR product was run on a 1% agarose gel, and amplicons of ~1450 bp were submitted for Sanger sequencing at Psomagen. Sequences were processed in Geneious Prime [20] by trimming the beginning and ends of reads to Q > 30, aligning forward and reverse reads using the MUSCLE alignment, and generating consensus sequences. NCBI BLASTN was used to identify the species of each sequence based on percent identity.

Isolates were tested in competitive assays against *Batrachochytrium dendrobatidis* (Bd) to determine each isolate's Bd-inhibitory potential (**Supplemental Table 1**). Bd zoospores, collected from filtered liquid culture and quantified using a hemocytometer, and bacterial isolates were co-cultured in microcosms containing 800 µL of 1% tryptone broth, 100 µL of bacterial isolate (OD_{600} = 0.1), and 100 µL of Bd zoospores (2 x 10^7 cells/mL). Microcosms were

incubated at 23°C for 72 hours. After incubation, cultures were centrifuged at 10,000 x g for 5 minutes to pellet cells, and then the cell-free supernatant (CFS) containing extracellular metabolites was separated by filtration using a 0.22 μm filter. A new culture of Bd (2 x 10^7 cells/mL) was grown in the CFS (n = 3 per isolate; 50 μL CFS and 50 μL Bd per well in a 96-well microplate) and incubated at 23°C for one week. Controls included both media and Bd alone. Absorbance was measured daily on a Biotech Synergy H1 microplate reader at 460 nm. Inhibition was calculated following the protocol in Barnes et al. [6]. In brief, the CFS and Bd replicates were averaged, and the change in optical density over four time points was compared to the growth of the Bd control to determine percent inhibition.

For this work, a pure culture of *Batrachochytrium dendrobatidis* (Bd, strain JEL423) was acquired from the Collection of Zoosporic Eufungi at the University of Michigan (CZEUM), and a pure culture of *Batrachochytrium salamandrivorans* (Bsal) was acquired from the Rollins-Smith Lab at Vanderbilt University.

Microcosm Assembly

From the sequenced isolates, ten species were chosen for use in synthetic microbial communities (SynComs; **Supplemental Table 1**). SynComs consisted of host-relevant proportions of seven species from the phylum Peusodomonadota (*Janthinobacterium lividum, Achromobacter denitrificans, Stenotrophomonas humi, Acinetobacter calcoaceticus, Citrobacter braakii, Buttiauxella sp.* 3AFRM03*,* and *Pseudomonas protegens*), two from the phylum Actinomycetota (*Microbacterium oxydans* and *Serratia fonticola),* and one from the phylum Bacteroidota (*Chryseobacterium indologenes*) suspended in M9 minimal medium supplemented with 1% porcine gastric mucin (type III; Sigma-Aldrich Cat. #M1778) and 0.5 mL 100X MEM

vitamins. Microcosms were assessed using low-volume, high-throughput assays [6] using a 5 x 2 factorial design (n = 5 replicates per treatment) consisting of five temperature treatments and two pathogen treatments (Bd or Bsal). Temperature treatments included: current northeast U.S. spring: 18°C [18], Bd's optimum (and Rochester's projected spring temperature): 20°C [10,21], hotspot structure: 29°C [16], proposed pond warming: 25°C [4], and Bsal's optimum: 15°C [12]. We also included Bd- and Bsal-only controls (n = 3), a SynCom-only control (i.e., bacterial community without pathogen; n = 3), and a media-only control (n = 3). Microcosms were incubated for eighteen days at each respective temperature with passaging to fresh media on days 6 and 12 in a 1:10 dilution. After passaging, the remaining SynCom volume was pelleted and stored in DNA/RNA Shield (Zymo Research) at -20°C until DNA/RNA extraction. Microcosms from days 0 and 18 were immediately spun down and stored in DNA/RNA Shield at -20°C.

Competition Assays

Cell-free supernatant (CFS) from each microcosm was collected using the methods described above. Cultures of Bd and Bsal were grown in the CFS of each microcosm (n = 3) and incubated at a single temperature: 23°C (Bd) [10] and 15°C (Bsal) [12] for one week to focus solely on the effects of the metabolites on pathogen growth. Measurements were taken daily on a Biotech Synergy H1 microplate reader at 460 nm. Inhibition was calculated as above by comparing growth of treatments to Bd/Bsal controls.

High-throughput 16S rRNA Sequencing

High-throughput 16S rRNA sequencing was used to track microbial composition over time (at 0, 6, 12, and 18 d). DNA was extracted using PrepMan Ultra according to the

manufacturer's protocol. The V4 region of the 16S rRNA gene was amplified using a set of dual-indexed primer pairs: 515F (5'- GTGCCAGCMGCCGCGGTAA - 3') and 806R (5'- GGACTACHVGGGTWTCTAAT - 3') [22]. Microbial DNA was amplified in duplicate 25 µL reactions: 12.5 µL of 2X Phusion Polymerase Master Mix (ThermoFisher), 1 µL each of 10 µM forward and reverse primers, and 2 µL of DNA. Amplifications were performed on a SimpliAmp thermal cycler under the following conditions: 98°C for 2 minutes for initial denaturation, 30 cycles of 98°C for 10 seconds, 55°C for 15 seconds, and 72°C for 1 minute, then 72°C for 10 minutes. Extraction kit and PCR controls were also included as negative sequencing controls, while the Day 0 samples were considered the positive controls (i.e., known abundance and composition). Duplicate reactions were pooled and run on gel electrophoresis (1% agarose) to determine successful amplification (i.e., amplicons of ~420 bp). Reactions were cleaned using AmpureXP magnetic beads (Beckman Coulter), quantified via Qubit fluorometer using the dsDNA High-Sensitivity kit (Invitrogen), and normalized to equal concentrations prior to library pooling into two pools with an equal number of samples. The final pools were sent for sequencing across two Illumina MiSeq runs using 2 x 250 bp paired-end sequencing at GeneWiz, Azenta Life Sciences (South Plainfield, NJ, USA).

Sequences were processed using QIIME2-2025.7 [23] on RIT's Research Computing Cluster. Primers and adapters were trimmed using cutadapt [24], and low-quality bases were trimmed (after mean $Q < 30$) before merging via DADA2 [25]. Reads were assigned to amplicon sequence variants (ASVs; sequence similarity 99%) using DADA2, and then taxonomy was assigned using a GTDB v2.6.0 classifier [26]. ASV and taxonomy tables were exported from QIIME2 for analysis in R.

Quantitative PCR

Bd and Bsal abundance in the microcosm was estimated using qPCR following Blooi et al. [22]. DNA from each microcosm was amplified in duplicate 20 µL reactions: 10 µL of PowerUp™ SYBR™ Green Master Mix (2X), 1 µL of 10 µM forward and reverse primers, and 2 µL of DNA. Amplifications were performed using a QuantStudio 3 real-time PCR system under the following conditions: 95°C for 2 minutes for initial denaturation, 50 cycles of 95°C for 15 seconds, and 60°C for 1 minute. Extraction kit and qPCR controls were included as negative controls, and DNA standards (n = 5, 1:10 serial dilution of DNA extracted from zoospores in pure culture) were considered positive controls.

Metatranscriptomic sequencing

Total RNA was extracted from Day 18 samples for both Bd and Bsal microcosms in the 29°C trial, Bd microcosms from the 20°C trial, and Bsal microcosms from the 15°C trial (n = 4; n_{total} = 16) using the RNeasy Mini Kit following protocols 3 and 7 from the RNAprotect Bacteria Reagent Handbook (Qiagen). Transcripts were sent to Novogene (Beijing, China) for metatranscriptomic sequencing with rRNA depletion on an Illumina NovaSeq6000 using 2 x 150 bp chemistry.

Raw metatranscriptome reads were transferred to KBase [27] for initial processing. Reads were filtered using the JGI filter protocol (BBTools v38.22) [28] with the remove RNA artifacts option and then trimmed using Trimmomatic (v.039) [29] with the sliding window size set to 3 and the minimum quality set to 30. Processed reads were then exported to the command line and aligned against a concatenated genome using Bowtie2 [30]. The concatenated genome consisted of the whole-genome sequences of the 10 bacteria in the microcosm (data unpublished),

196 annotated using DRAM [31]. The “very sensitive” preset was used for the most accurate
197 alignment. Feature counts were generated from aligned reads and exported into R for analysis.
198
199 *Statistical Analysis*
200 All post-QIIME2 analyses were performed in R v. 4.18 [32]. Taxonomic, metadata, and
201 ASV datasets were merged using the phyloseq package [33]. ASVs without phylum annotation
202 or those with low prevalence (defined as <30 reads and present in <5% of samples, as these
203 likely represented sequencing errors and not true microbes in the microcosm) were removed.
204 Alpha diversity was calculated using three metrics: evenness, Shannon diversity, and Chao1, and
205 analyzed via ANOVA. Community composition was measured using Bray-Curtis dissimilarities
206 and weighted Unifrac calculated on log(x+1)-transformed ASV counts. This transformation
207 helps to account for the effect of dominant versus rare species and allows the retention of zero
208 abundances as zeros [34]. Homogeneity of group dispersions was calculated with betadispers,
209 and PERMANOVA was used to assess significant differences in composition among treatments
210 using the vegan package [35], followed by post hoc pairwise comparisons using pairwise.adonis
211 [36]. Non-metric Multidimensional Scaling (NDMS) and relative abundance plots were used to
212 visualize community composition patterns across treatments. Differential abundance analysis
213 between temperature trials was compared using the ANCOMBC package [37]. All visualizations
214 were created using ggplot2 [38].
215 Metatranscriptomes were analyzed using the DESeq2 package [39]. Differentially
216 expressed genes were identified by filtering for an adjusted p-value < 0.05 and a log fold change
217 greater than one. Normalized counts were extracted, and differential expression was visualized
218 both with a PCoA and heatmap. Betadispersion was measured using betadispers [35] to

219 determine homogeneity of expression within temperature trials. Heatmaps were created using the
220 ggplot2 package [38]. A literature search was conducted to generate a list of genes of interest
221 (i.e., those associated with microbe-microbe interactions, mucin utilization, heat stress/shock,
222 and chitin binding (the main component of fungal cell walls); **Supplemental Data Table 1**).
223 This list was then used to filter differentially expressed genes identified by DESeq2 analysis.
224
225 **Results**
226 *Temperature and time restructure community composition without altering alpha diversity*
227 Following sequencing and quality filtering (272 samples; mean = 32,825 reads/sample),
228 we evaluated synthetic community (SynCom) dynamics across thermal regimes. Consistent with
229 our expectations, temperature did not significantly alter bacterial alpha diversity, as measured by
230 Shannon diversity or Chao1. However, in SynComs containing Bd, alpha diversity as measured
231 by evenness was significantly affected by temperature ($F_{(4,85)}$= 3.07, p = 0.02; **Supplemental**
232 **Tables 2-3**; S**upplemental Figure 1; Supplemental Data Tables 2-3**). The interaction between
233 temperature and time was also shown to significantly affect alpha diversity in those SynComs
234 (Day: $F_{(1,85)}$= 28.25, p= 8.47E-07; Interaction: $F_{(4,85)}$= 2.51, p= 0.047; **Supplemental Tables 2-**
235 **3**; S**upplemental Figure 1; Supplemental Data Tables 2-3**). Community evenness exhibited a
236 decreasing trend at higher temperatures (median Bd SynComs: 15°C = 0.872, 29°C = 0.737;
237 median Bsal SynComs: 15°C = 0.77, 29°C = 0.75), whereas Chao1 estimates increased slightly
238 due to the increased relative weight of rare taxa.
239 In contrast to alpha diversity, bacterial community composition was significantly
240 influenced by temperature (Bd: $F_{(4,20)}$ = 4.25, R^2 = 0.06, p = 0.002; Bsal: $F_{(3,57)}$ = 4.3, R^2 = 0.05,
241 p = 0.02), time (Bd: $F_{(3,20)}$ = 58.80, R^2 = 0.63, p = 0.001; Bsal: R^2 = 0.69, $F_{(3,57)}$ = 79.35, p =

0.001), and their interaction (Bd: $F_{(11,20)} = 2.35$, $R^2 = 0.09$, $p = 0.006$; Bsal: $F_{(12, 57)} = 2.89$, $R^2 = 0.10$, $p = 0.001$; **Figure 2C-D, Supplemental Tables 4-5**, **Supplemental Figures 2-3**). Differential abundance analysis revealed taxon-specific thermal responses. Isolates belonging to Burkholderiaceae significantly increased in relative abundance at elevated temperatures in Bd microcosms compared to the 20°C control (25°C: $\log_2FC = 0.79$, $p_{adj} = 0.01$; 29°C: $\log_2FC = 0.88$, $p_{adj} = 0.02$; **Supplemental Figure 4**). Conversely, in Bsal microcosms, Mycobacteriaceae isolates significantly decreased at elevated temperatures relative to the 15 °C control (25°C: $\log_2FC = -1.68$, $p_{adj} = 0.02$; 29°C: $\log F_2C = -1.54$, $p_{adj} = 0.04$; **Supplemental Figure 4**), dropping below detection limits in several temperature treatments by day 18 (asterisks in **Figure 3A-B**). Calculating pairwise compositional dissimilarity between initial (day 0) and final (day 18) microcosms confirmed that community trajectories diverged more substantially over time under elevated warming (**Supplemental Figure 5**).

Temperature exerts pathogen-specific effects on chytrid abundance and inhibition

We next evaluated how thermal treatments influenced pathogen suppression and overall fungal load at the final time point. Temperature significantly altered Bsal inhibition, but not Bd inhibition (Bsal: $F_{(4,20)} = 4.469$, $R^2 = 0.47$, $p = 0.01$; Bd: $F_{(4,20)} = 2.2$, $R^2 = 0.31$, $p = 0.11$; **Figure 2 A-B**, **Supplemental Tables 6-7**). Similarly, total pathogen abundance varied significantly across temperatures on the final day of the experiment, primarily for Bsal (**Supplemental Table 7**). Total pathogen abundance was highest at 25°C, corresponding with lower microbiome inhibition capacity. Microcosms incubated at baseline thermal optima (Bd: 20°C; Bsal: 15°C) maintained higher pathogen loads on day 18 compared to extreme warming treatments (29°C), consistent with our hypotheses, though this trend was not statistically significant. Lowest

pathogen abundances were observed in the 29°C-Bd and 20°C-Bsal treatments (**Supplemental Figure 6**). Temporal dynamics also diverged between pathogens: Bsal microcosms maintained elevated chytrid abundance until day 6 before experiencing a steep decline, whereas Bd loads dropped sharply at day zero across all treatments except the 20°C control (**Supplemental Figure 7**). Pathogen abundance was significantly affected by temperature, time, and the interaction between the two in Bd SynComs (Time: $F_{(4,130)}$= 24.4, p = 1.37e-12; Temperature: $F_{(3,130)}$= 9.7, p = 6.73e-07; Interaction: $F_{(12,130)}$= 4.78, p = 1.89e-06) but not in Bsal SynComs, where abundance was only significantly affected by time (Time: $F_{(12,80)}$= 5.91, p = 0.0011; Temperature: $F_{(3,80)}$= 0.41, p = 0.8; Interaction: $F_{(12,80)}$= 0.7, p = 0.74; **Supplemental Tables 8-9; Supplemental Data Table 4)**.

Elevated temperature constrains transcriptomic diversity and downregulates bacterial competition pathways

In comparisons of the metatranscriptome at day 18, total functional richness decreased at elevated temperatures; all genes expressed in the 29°C treatment represented a subset of those active at lower temperatures (**Figure 4A, Supplemental Figures 8-10**). Ordination and PERMANOVA analysis confirmed that community-wide transcriptomic profiles significantly diverged by temperature (Bd: $F_{(1,6)}$ = 3.49, R^2 = 0.37, p = 0.04; Bsal: $F_{(1,5)}$ = 5.37, R^2 = 0.52, p = 0.04; **Supplemental Table 10**), contracting into a highly homogeneous functional state at 29°C (**Figure 4B-C**). Global differential expression profiling revealed that downregulated transcripts at 29°C were heavily enriched for pathways involved in bacterial motility, nutrient acquisition, and protein secretion (**Supplemental Figures 9-10**).

Taxon-resolved transcript mapping revealed that functional shifts were driven by distinct subsets of the synthetic community rather than uniform expression across all members. Transcripts encoding secretion systems mapped primarily to *Achromobacter denitrificans*, *Citrobacter braakii*, *Stenotrophomonas humi*, and *Janthinobacterium lividum*. Pathways governing spatial dynamics and interbacterial communication—specifically motility/adhesion and quorum sensing—were expressed predominantly by *J. lividum*, *Pseudomonas protegens*, *A. denitrificans*, and *Serratia fonticola*, with chemotaxis transcripts mapping specifically to *S. humi* and *S. fonticola*. Additionally, iron-siderophore transport genes mapped to *P. protegens*, *C. braakii*, and *S. fonticola*, while vitamin B biosynthesis and transport mapped to *A. denitrificans*, *S. fonticola*, *P. protegens*, and *Buttiauxella* sp.

We also evaluated specific candidate genes hypothesized to mediate Bd/Bsal inhibition. These genes included those associated with mucin utilization, heat shock, stress response, and chitin degradation (the main component of fungal cell walls). Of the genes of interest, seven out of sixteen unique functions were found. In both Bd and Bsal microcosms, extreme warming (29°C) led to significant downregulation of genes governing chemical sensing and interbacterial warfare. Specifically, KOs associated with chemotactic adaptation, including the global thermosensor protein H-NS (K03746) in Bd microcosms and the CheB/CheR fusion protein (K13924) in Bsal microcosms, were downregulated. Similarly, structural components of type VI secretion systems (T6SS; Bd: K11914 and K13942; Bsal: K11914), which mediate contact-dependent interbacterial competition, were downregulated at 29°C. Pathogen-specific responses were also observed at 29°C: Bd microcosms exhibited downregulation of cobalamin (vitamin B12) biosynthetic genes (K21135), whereas Bsal microcosms showed downregulation of type IV

secretion system (T4SS) components (K12071) alongside marked upregulation of heat-shock molecular chaperones (K03089, K04043).

Discussion

The chytrid panzootic is a devastating threat to global amphibian diversity, a group already severely imperiled by habitat loss and climate change [2]. While artificial environmental warming has been proposed as a conservation strategy to suppress chytridiomycosis, its indirect impacts on the host-associated microbiome–a critical line of immune defense–remain poorly understood [4]. Using synthetic microbial communities (SynComs) across controlled thermal regimes, this study reveals that while taxonomic structure exhibits apparent resilience to warming, microbial functional capacity undergoes substantial temperature-induced change.

Decoupling of taxonomic stability and functional expression under warming

Environmental temperature and temporal succession interact to dynamically restructure microbial communities during chytrid infection. In our system, synthetic communities remained in a transient compositional state through day 18 rather than reaching an ecological equilibrium. These findings align with other studies exploring the interaction between Bd/Bsal pathogenicity and temperature [7,8,12,16,17]. From a community assembly perspective, acute environmental stressors like warming (29°C) exert strong deterministic selection on microbial expression before driving structural turnover or species sorting. Crucially, while overall alpha diversity at day 18 appeared resilient across temperature shifts, endpoint metatranscriptomic profiling revealed temperature-dependent functional shifts, including the widespread downregulation of genes associated with microbial competition at 29°C. This decoupling highlights a key ecological

mismatch in microbiome dynamics: large functional shifts can occur with environmental change without being reflected by major shifts in taxonomic richness or community turnover [40–43]. This suggests that at least in the short term, amphibian-associated bacteria can cope with warming by shifting their functional gene use (i.e., functional plasticity) rather than drastically changing community membership. This insight is vital for applied conservation, as it reveals that broad taxonomic monitoring can mask hidden metabolic collapse. The success of probiotic treatments or thermal mitigation cannot solely be determined by microbial survival, but should also verify that protective metabolic pathways remain actively expressed under field conditions.

While microbial alpha diversity was relatively stable, beta diversity patterns revealed that thermal stress destabilized community assembly over time. Pairwise compositional dissimilarity between day 0 and day 18 confirmed that community trajectories diverged far more substantially under elevated warming than at ambient temperatures, consistent with the "Anna Karenina Principle" [44]. This temporal divergence was driven by highly deterministic population shifts– most notably the complete exclusion of Mycobacteriaceae in many treatments by day 18. Conversely, Burkholderiaceae (in Bd microcosms) and Pseudomonadaceae/Sphingobacteriaceae (in Bsal microcosms) expanded at elevated temperatures, demonstrating that thermal stress acts as an environmental filter that selectively alters key protective lineages even when broad diversity metrics remain static. Relying solely on taxonomic profiling at experimental endpoints risks misinterpreting transient states as stable, functional equilibria [45,46]. Evaluating functional gene expression alongside long-term temporal assembly is therefore essential to determine whether thermal mitigation strategies push protective host microbiomes toward alternative stable states or loss of protective capacity.

Thermal stress forces a metabolic trade-off between heat survival and interbacterial warfare

Under extreme thermal stress (29°C), synthetic skin communities undergo a widespread functional shift, prioritizing immediate physiological survival over competition. Bacteria reallocated their energy budget toward cellular repair chaperones (*dnaK/groEL*; K03089, K04043) while suppressing high-energy molecular weapons, including structural components of Type VI secretion systems (T6SS; K11914, K13942). Importantly, taxon-resolved transcript mapping demonstrated that this functional disarming was driven by specific community members rather than a uniform population response (as has been observed in the rhizosphere [47] and tadpole gut [48]). Transcripts encoding T6SS mapped overwhelmingly to *Achromobacter denitrificans*, *Citrobacter braakii*, *Stenotrophomonas humi*, and *Janthinobacterium lividum*, indicating that warming selectively disarms the primary competitive members of the SynCom.

Additionally, chemotaxis adaptors and global thermosensors, such as H-NS (K03746) in Bd microcosms and CheB/CheR (K13924) in Bsal microcosms, were significantly downregulated at 29°C. Because H-NS regulates DNA-binding conformation in response to thermal cues [49,50], its suppression directly impacts flagellar motility, adhesion, and biofilm formation, which were predominantly expressed by *Janthinobacterium lividum*, *Pseudomonas protegens*, and *Serratia fonticola*. Furthermore, candidate genes directly implicated in fungal cell wall degradation and host colonization, including chitinases and mucin utilization pathways, were among the suppressed functions. This systematic downregulation demonstrates that warming alters not only baseline bacterial metabolism, but specifically disables the machinery required for spatial organization, nutrient competition, and pathogen inhibition.

Pathogen-specific responses and off-target impacts of thermal mitigation

Environmental warming exerted divergent impacts on Bd versus Bsal abundance and inhibition, reflecting fundamental differences in pathogen thermal ecology that correspond to metatranscriptomic reconfigurations. At the experimental endpoint, temperature significantly reduced Bsal inhibition capacity: Bsal abundance peaked at 25°C (where microbial inhibition was markedly reduced) whereas abundance was lowest under extreme warming (29°C). Conversely, Bd inhibition remained relatively stable across temperatures, with lowest fungal loads observed at 29°C. While higher temperatures slow chytrid growth and bolster host immune physiology [4,8,10–12,16,17,51–54], our findings demonstrate an unintended environmental trade-off: warming inadvertently impairs protective bacterial functions even when fungal loads are reduced.

Crucially, the concurrent contraction of overall functional richness and upregulation of heat-shock chaperones at 29°C indicate that thermal stress directly constrains bacterial metabolic capacity, altering microbial functionality regardless of pathogen density. Because Bsal is a cold-adapted pathogen with a lower thermal optimum (15°C) than Bd (20°C) [3,10,11], environmental warming pushes Bsal past its thermal threshold faster than Bd. However, this thermal divergence induced distinct functional disruptions in the associated microbiome: Bd microcosms exhibited marked downregulation of cobalamin (vitamin B12) biosynthesis (K21135), whereas Bsal microcosms downregulated Type IV secretion systems (T4SS; K12071). Because key metabolic functions, such as iron-siderophore acquisition and B-vitamin transport, were partitioned among specialized taxa like *P. protegens*, *Buttiauxella* sp., and *S. fonticola*, thermal impairment of these specific pathways alters the nutritional microenvironment. Because chytrids generally lack a complete de novo cobalamin synthesis pathway [55], they scavenge B12 from commensal bacteria. Thus, downregulation of this pathway among bacteria directly starves Bd of a

fundamental co-factor necessary for cellular respiration, zoospore germination, and growth. At the same time, impairment of bacterial iron-siderophore acquisition could relieve iron competition in favor of the pathogen [56,57]. Loss of these nutrients can also indirectly affect Bd via collapse of the bacterial cross-feeding network wherein bacteria rely on these donor nutrients for production of secondary metabolites (many of which are anti-fungal compounds) [58]. This is in contrast to observations in Bsal microcosms which suffered from structural/weaponry degradation. Ultimately, these distinct metabolic disruptions mean that environmental warming may weaken host defense through pathogen-specific ecological pathways indicating that disease management may not be able to rely on a "one-size-fits-all" thermal mitigation strategy.

Implications for amphibian conservation and SynCom engineering

The integration of synthetic communities and metatranscriptomics provides a high-resolution framework for disentangling complex microbe-microbe and microbe-environment interactions. While SynComs allow precise mechanistic insights into bacterial trade-offs, fully translating these findings to conservation requires evaluating these dynamics in vivo. Host epithelial secretions, mucosal immunity, and behavioral thermoregulation undoubtedly modulate microbiome expression and community assembly [59–61]. Future research combining multi-omics with host-pathogen infection trials across extended temporal scales will be vital for defining stable, protective community states. Ultimately, accounting for functional trade-offs in the microbiome is essential to ensure that thermal mitigation strategies do not inadvertently dismantle the mucosal defenses of amphibians.

Funding

ET was funded by the RIT Emerson Summer Undergraduate Research Fellowship, the Steven M. Wear Endowed Graduate Fellowship, and the Rochester Academy of Science Student Grant. EMB was funded by the Arnold and Mabel Beckman Foundation.

Acknowledgements

We thank William Goyette for his assistance with aspects of the microcosm assembly and competition assays. We thank Dr. Elena Lopez-Peredo and Dr. Elizabeth Dicesare for feedback on initial drafts of this research.

Data Availability

All sequence data associated with this research is available on NCBI's Sequence Read Archive under BioProject PRJNA1529745 (set to release publicly upon publication). All code and non-sequence data files needed to reproduce the analysis are available in the project's GitHub repository: https://github.com/MEGA-Lab-RIT/temperature-sal-microbes.

References

1. AmphibiaWeb | Home. n.d. https://amphibiaweb.org/index.html (8 Aug. 2026, date last accessed).

2. Luedtke JA, Chanson J, Neam K *et al.* Ongoing declines for the world's amphibians in the face of emerging threats. *Nature* 2023;**622**(7982):308–14. https://doi.org/10.1038/s41586-023-06578-4.

3. Sluijs AS van der, Martel A, Asselberghs J *et al.* Expanding Distribution of Lethal Amphibian Fungus Batrachochytrium salamandrivorans in Europe. *Emerg Infect Dis* 2016;**22**(7):1286. https://doi.org/10.3201/eid2207.160109.

4. Bletz MC, Grant EHC, DiRenzo G. Quantitative support for the benefits of proactive management for wildlife disease control. *Conserv Biol* 26 Aug. 2024:e14363. https://doi.org/10.1111/cobi.14363.

5. Grear DA, Mosher BA, Richgels KLD *et al.* Evaluation of regulatory action and surveillance as preventive risk-mitigation to an emerging global amphibian pathogen *Batrachochytrium salamandrivorans* (Bsal). *Biol Conserv* 2021;**260**:109222. https://doi.org/10.1016/j.biocon.2021.109222.

6. Barnes EM, Kutos S, Naghshineh N *et al.* Assembly of the amphibian microbiome is influenced by the effects of land-use change on environmental reservoirs. *Environ Microbiol* 2021;**23**(8):4595–611. https://doi.org/10.1111/1462-2920.15653.

7. Turner A, Wassens S, Heard G *et al.* TEMPERATURE AS A DRIVER OF THE PATHOGENICITY AND VIRULENCE OF AMPHIBIAN CHYTRID FUNGUS BATRACHOCHYTRIUM DENDROBATIDIS: A SYSTEMATIC REVIEW. *J Wildl Dis* 2021;**57**(3). https://doi.org/10.7589/JWD-D-20-00105.

8. Robak MJ, Saenz V, Cortie E de *et al.* Effects of temperature on the interaction between amphibian skin bacteria and Batrachochytrium dendrobatidis. *Front Microbiol* 2023;**14**. https://doi.org/10.3389/fmicb.2023.1253482.

9. Pottier P, Lin HY, Oh RRY *et al.* A comprehensive database of amphibian heat tolerance. *Sci Data* 2022;**9**(1):600. https://doi.org/10.1038/s41597-022-01704-9.

10. Rollins-Smith LA, Le Sage EH. Batrachochytrium fungi: stealth invaders in amphibian skin. *Curr Opin Microbiol* 2021;**61**:124–32. https://doi.org/10.1016/j.mib.2021.04.002.

11. Kelly M, Pasmans F, Muñoz JF *et al.* Diversity, multifaceted evolution, and facultative saprotrophism in the European Batrachochytrium salamandrivorans epidemic. *Nat Commun* 2021;**12**(1):6688. https://doi.org/10.1038/s41467-021-27005-0.

12. Carter ED, Bletz MC, Le Sage M *et al.* Winter is coming–Temperature affects immune defenses and susceptibility to Batrachochytrium salamandrivorans. *PLOS Pathog* 2021;**17**(2):e1009234. https://doi.org/10.1371/journal.ppat.1009234.

13. Buttimer S, Moura-Campos D, Greenspan SE *et al.* Skin microbiome disturbance linked to drought-associated amphibian disease. *Ecol Lett* 2024;**27**(1):e14372. https://doi.org/10.1111/ele.14372.

14. Greenspan SE, Migliorini GH, Lyra ML *et al.* Warming drives ecological community changes linked to host-associated microbiome dysbiosis. *Nat Clim Change* 2020;**10**(11):1057–61. https://doi.org/10.1038/s41558-020-0899-5.

15. Kueneman JG, Bletz MC, McKenzie VJ *et al.* Community richness of amphibian skin bacteria correlates with bioclimate at the global scale. *Nat Ecol Evol* 2019;**3**(3):381–9. https://doi.org/10.1038/s41559-019-0798-1.

16. Waddle AW, Clulow S, Aquilina A *et al.* Hotspot shelters stimulate frog resistance to chytridiomycosis. *Nature* 2024;**631**(8020):344–9. https://doi.org/10.1038/s41586-024-07582-y.

17. Hettyey A, Ujszegi J, Herczeg D *et al.* Mitigating Disease Impacts in Amphibian Populations: Capitalizing on the Thermal Optimum Mismatch Between a Pathogen and Its Host. *Front Ecol Evol* 2019;**7**:254. https://doi.org/10.3389/fevo.2019.00254.

18. Rochester Climate, Weather By Month, Average Temperature (New York, United States) - Weather Spark. n.d. https://weatherspark.com/y/21245/Average-Weather-in-Rochester-New-York-United-States-Year-Round (27 Jan. 2025, date last accessed).

19. Miller CS, Handley KM, Wrighton KC *et al.* Short-Read Assembly of Full-Length 16S Amplicons Reveals Bacterial Diversity in Subsurface Sediments. *PLOS ONE* 2013;**8**(2):e56018. https://doi.org/10.1371/journal.pone.0056018.

20. Kearse M, Moir R, Wilson A *et al.* Geneious Basic: An integrated and extendable desktop software platform for the organization and analysis of sequence data. *Bioinformatics* 2012;**28**(12):1647–9. https://doi.org/10.1093/bioinformatics/bts199.

21. How climate change has affected Rochester. *RochesterFirst* 15 Nov. 2023. https://www.rochesterfirst.com/winter-weather-outlook/how-climate-change-has-affected-rochester/ (6 Dec. 2024, date last accessed).

22. Blooi M, Pasmans F, Longcore JE *et al.* Duplex real-time PCR for rapid simultaneous detection of Batrachochytrium dendrobatidis and Batrachochytrium salamandrivorans in Amphibian samples. *J Clin Microbiol* 2013;**51**(12):4173–7. https://doi.org/10.1128/JCM.02313-13.

23. Bolyen E, Rideout JR, Dillon MR *et al.* Reproducible, interactive, scalable and extensible microbiome data science using QIIME 2. *Nat Biotechnol* 2019;**37**(8):852–7. https://doi.org/10.1038/s41587-019-0209-9.

24. Martin M. Cutadapt removes adapter sequences from high-throughput sequencing reads. *EMBnetJournal* 2011;**17**(1):10–2. https://doi.org/10.14806/ej.17.1.200.

25. Callahan BJ, McMurdie PJ, Rosen MJ *et al.* DADA2: High-resolution sample inference from Illumina amplicon data. *Nat Methods* 2016;**13**(7):581–3. https://doi.org/10.1038/nmeth.3869.

26. Parks DH, Chuvochina M, Rinke C *et al.* GTDB: an ongoing census of bacterial and archaeal diversity through a phylogenetically consistent, rank normalized and complete genome-based taxonomy. *Nucleic Acids Res* 2022;**50**(D1):D785–94. https://doi.org/10.1093/nar/gkab776.

27. Arkin AP, Cottingham RW, Henry CS *et al.* KBase: The United States Department of Energy Systems Biology Knowledgebase. *Nat Biotechnol* 2018;**36**(7):566–9. https://doi.org/10.1038/nbt.4163.

28. Bushnell B, Rood J, Singer E. BBMerge – Accurate paired shotgun read merging via overlap. *PLOS ONE* 2017;**12**(10):e0185056. https://doi.org/10.1371/journal.pone.0185056.

29. Bolger AM, Lohse M, Usadel B. Trimmomatic: a flexible trimmer for Illumina sequence data. *Bioinformatics* 2014;**30**(15):2114–20. https://doi.org/10.1093/bioinformatics/btu170.

30. Langmead B, Salzberg SL. Fast gapped-read alignment with Bowtie 2. *Nat Methods* 2012;**9**(4):357–9. https://doi.org/10.1038/nmeth.1923.

31. Shaffer M, Borton MA, McGivern BB *et al.* DRAM for distilling microbial metabolism to automate the curation of microbiome function. *Nucleic Acids Res* 2020;**48**(16):8883–900. https://doi.org/10.1093/nar/gkaa621.

32. R Core Team. *R: A Language and Environment for Statistical Computing*. R Foundation for Statistical Computing, Vienna, Austria., 2025. https://www.R-project.org.

33. McMurdie PJ, Holmes S. phyloseq: An R Package for Reproducible Interactive Analysis and Graphics of Microbiome Census Data. *PLOS ONE* 2013;**8**(4):e61217. https://doi.org/10.1371/journal.pone.0061217.

34. Serrana JM, Watanabe K. Sediment-associated microbial community profiling: sample pre-processing through sequential membrane filtration for 16S rRNA amplicon sequencing. *BMC Microbiol* 2022;**22**(1):33. https://doi.org/10.1186/s12866-022-02441-0.

35. Oksanen J, Simpson GL, Blanchet FG *et al.* vegan: Community Ecology Package. 6 Sept. 2001, 2.6-10. https://doi.org/10.32614/CRAN.package.vegan.

36. Martinez P. *pairwiseAdonis: Pairwise Multilevel Comparison Using Adonis*, R, version 0.4. 1 Oct. 2017, 2020. https://github.com/pmartinezarbizu/pairwiseAdonis (10 Apr. 2026, date last accessed).

37. Lin H, Peddada SD. Multigroup analysis of compositions of microbiomes with covariate adjustments and repeated measures. *Nat Methods* 2024;**21**(1):83–91. https://doi.org/10.1038/s41592-023-02092-7.

38. Create Elegant Data Visualisations Using the Grammar of Graphics. n.d. https://ggplot2.tidyverse.org/ (9 Aug. 2026, date last accessed).

39. Love MI, Huber W, Anders S. Moderated estimation of fold change and dispersion for RNA-seq data with DESeq2. *Genome Biol* 2014;**15**(12):550. https://doi.org/10.1186/s13059-014-0550-8.

40. Bennett AE, Kelsey S, Saup C *et al.* Selenium alters the gene content but not the taxonomic composition of the soil microbiome. *Springer Nat* 2024;**19**(92). https://doi.org/https://doi.org/10.1186/s40793-024-00641-x.

41. Poyntner C, Täumer J, Dahl MB *et al.* Changes in the (micro-)biome structure and function of two forest sites in the Alps at different elevations and seasons using metatranscriptomics. *Appl Soil Ecol* 2026;**223**:107050. https://doi.org/10.1016/j.apsoil.2026.107050.

42. Louca S, Parfrey LW, Doebeli M. Decoupling function and taxonomy in the global ocean microbiome. *Science* 2016;**353**(6305):1272–7. https://doi.org/10.1126/science.aaf4507.

43. Wright RJ, Gibson MI, Christie-Oleza JA. Understanding microbial community dynamics to improve optimal microbiome selection. *Microbiome* 2019;**7**(1):85. https://doi.org/10.1186/s40168-019-0702-x.

44. Zaneveld JR, McMinds R, Vega Thurber R. Stress and stability: applying the Anna Karenina principle to animal microbiomes. *Nat Microbiol* 2017;**2**(9):17121. https://doi.org/10.1038/nmicrobiol.2017.121.

45. Özkurt E. Experimental systems are essential for strengthening ecological modeling of microbiomes beyond observational data. *mSystems* n.d.;**10**. https://journals.asm.org/doi/10.1128/msystems.01745-24 (2 Sept. 2026, date last accessed).

46. Flores C, Millard S, Seekatz AM. Bridging Ecology and Microbiomes: Applying Ecological Theories in Host-associated Microbial Ecosystems. *Curr Clin Microbiol Rep* 2025;**12**(1):9. https://doi.org/10.1007/s40588-025-00246-z.

47. Xu L, Dong Z, Chiniquy D *et al.* Genome-resolved metagenomics reveals role of iron metabolism in drought-induced rhizosphere microbiome dynamics. *Nat Commun* 2021;**12**(1):3209. https://doi.org/10.1038/s41467-021-23553-7.

48. Fontaine SS, Kohl KD. The microbiome buffers tadpole hosts from heat stress: a hologenomic approach to understand host–microbe interactions under warming. *J Exp Biol* 2023;**226**(1):jeb245191. https://doi.org/10.1242/jeb.245191.

49. Cooper C, Legood S, Wheat RL *et al.* H-NS is a bacterial transposon capture protein. *Nat Commun* 2024;**15**(1):7137. https://doi.org/10.1038/s41467-024-51407-5.

50. Ono S, Goldberg MD, Olsson T *et al.* H-NS is a part of a thermally controlled mechanism for bacterial gene regulation. *Biochem J* 2005;**391**(2):203–13. https://doi.org/10.1042/BJ20050453.

51. Gray MJ, Carter ED, Piovia-Scott J *et al.* Broad host susceptibility of North American amphibian species to Batrachochytrium salamandrivorans suggests high invasion potential and biodiversity risk. *Nat Commun* 2023;**14**(1):3270. https://doi.org/10.1038/s41467-023-38979-4.

52. Kásler A, Holly D, Herczeg D *et al.* Chytridiomycosis and climate change: exposure to *Batrachochytrium dendrobatidis* and mild winter conditions do not increase mortality in juvenile agile frogs during hibernation. *Anim Conserv* 2023;**26**(5):654–62. https://doi.org/10.1111/acv.12851.

53. Lindauer AL, Maier PA, Voyles J. Daily fluctuating temperatures decrease growth and reproduction rate of a lethal amphibian fungal pathogen in culture. *BMC Ecol* 2020;**20**(1):18. https://doi.org/10.1186/s12898-020-00286-7.

54. Winters DM, Wilson E, Coster SS *et al.* Integrating Population Genetics With Long-Term Environmental Monitoring to Evaluate and Guide Vernal Pool Creation for Amphibian Conservation. *Ecol Evol* 2024;**14**(10):e70431. https://doi.org/10.1002/ece3.70431.

55. Orłowska M, Steczkiewicz K, Muszewska A. Utilization of Cobalamin Is Ubiquitous in Early-Branching Fungal Phyla. *Genome Biol Evol* 2021;**13**(4):evab043. https://doi.org/10.1093/gbe/evab043.

56. Wax N, Walke JB, Haak DC *et al.* Comparative genomics of bacteria from amphibian skin associated with inhibition of an amphibian fungal pathogen, Batrachochytrium dendrobatidis. *PeerJ* 2023;**11**:e15714. https://doi.org/10.7717/peerj.15714.

57. Wang C, Kuzyakov Y. Mechanisms and implications of bacterial–fungal competition for soil resources. *ISME J* 2024;**18**(1):wrae073. https://doi.org/10.1093/ismejo/wrae073.

58. Morgan BG, Warren P, Mewis RE *et al.* Bacterial dominance is due to effective utilisation of secondary metabolites produced by competitors. *Sci Rep* 2020;**10**(1):2316. https://doi.org/10.1038/s41598-020-59048-6.

59. Colombo BM, Scalvenzi T, Benlamara S *et al.* Microbiota and Mucosal Immunity in Amphibians. *Front Immunol* 2015;**6**. https://doi.org/10.3389/fimmu.2015.00111.

60. Kröner L, Lötters S, Hopp MT. Insights into caudate amphibian skin secretions with a focus on the chemistry and bioactivity of derived peptides. *Biol Chem* 2024;**405**(9–10):641–60. https://doi.org/10.1515/hsz-2024-0035.

61. Rollins-Smith LA. The future of amphibian immunology: Opportunities and challenges. *Dev Comp Immunol* 2024;**160**:105237. https://doi.org/10.1016/j.dci.2024.105237.

62. Brucker RM, Harris RN, Schwantes CR *et al.* Amphibian Chemical Defense: Antifungal Metabolites of the Microsymbiont Janthinobacterium lividum on the Salamander Plethodon cinereus. *Springer Nat* 2008;**34**:1422–9. https://doi.org/https://doi.org/10.1007/s10886-008-9555-7.

Figure Captions

Figure 1. Experimental system overview. A. Symbiotic bacteria can indirectly protect the host by outcompeting or inhibiting Bd/Bsal growth on host skin. Adapted from Brucker et al. 2008 [62]. **B**. The system can be impacted by increased temperatures from both climate change and proposed conservation methods. Increased temperature can result in elevated physiological stress in amphibian hosts, decline in chytrid growth rates, and shifts in community composition and gene expression of the host microbiome. Experiments in this paper cover only the interactions between chytrid, temperature, and the microbiome, excluding the host.

Figure 2. Effect of temperature on pathogen inhibition and community composition. A-B. Percent inhibition on Day 18 for Bd (**A**) and Bsal (**B**) in each temperature trial as measured by competition assay. Median and interquartile range (IQR) with whiskers extending to 1.5X IQR, with outliers denoted as solid black points and all points as gray points. Inhibition was analyzed via one-way ANOVA (Bd: $F_{(4,20)} = 2.2$, $p = 0.11$; Bsal: $F_{(4,20)} = 4.5$, $p = 0.01$). **C-D**. Community composition was examined via PERMANOVA on weighted UniFrac distances for communities with Bd (**C**) or Bsal (**D**). Time is represented by shape and temperature represented by color. Time (Bd: $F_{(3,20)} = 58.8$, $p = 0.001$; Bsal: $F_{(3,57)} = 79.35$, $p = 0.001$), temperature (Bd: $F_{(4,20)} = 2.2$, $p = 0.11$; Bsal: $F_{(4,57)} = 4.3$, $p = 0.02$), and their interaction (Bd: $F_{(11,20)} = 2.4$, $p = 0.006$; Bsal: $F_{(12,57)} = 2.4$, $p = 0.001$) significantly influence community composition.

Figure 3. Change in community composition relative to pathogen optima. A-B. Relative abundance of bacteria in Bd (**A**) and Bsal (**B**) microcosms by both temperature and time. Samples are ordered by time within each temperature subset, with each bar representing individual replicates. The family Mycobacteriaceae disappears over time; the time point at which its abundance reached zero is denoted with an asterisk. **C-D**. Change in community composition between experimental temperatures vs. pathogen thermal optima (as measured by Bray-Curtis dissimilarity) in microcosms containing Bd (**C**) or Bsal (**D**). Based on the literature, the thermal optimum for Bd is 20°C and Bsal is 15°C.

Figure 4. Differences in the metatranscriptomic profile of microcosms with pathogen and temperature. A. Venn diagram comparing the difference in the total number of unique transcripts identified within each experimental group. Genes expressed within each experimental group and shared between groups represent a percentage of the total number of genes expressed during the trial. **B-C**. PCoA of gene expression of microcosms containing Bd (**B**) and Bsal (**C**). No ellipse is shown for the 29°C trial with Bsal since $n < 4$ due to poor RNA quality of one replicate.

Figure 5. Expression patterns of genes of interest identified via metatranscriptomic sequencing. Differentially expressed genes within microcosms with Bd (**A**) or Bsal (**B**) were

filtered by KO number to represent only those that possess functions associated with fungal resistance, mucin utilization, or heat stress/heat shock. Gene counts are depicted as log-transformed, DESeq2-normalized.

662 **Figure 1**

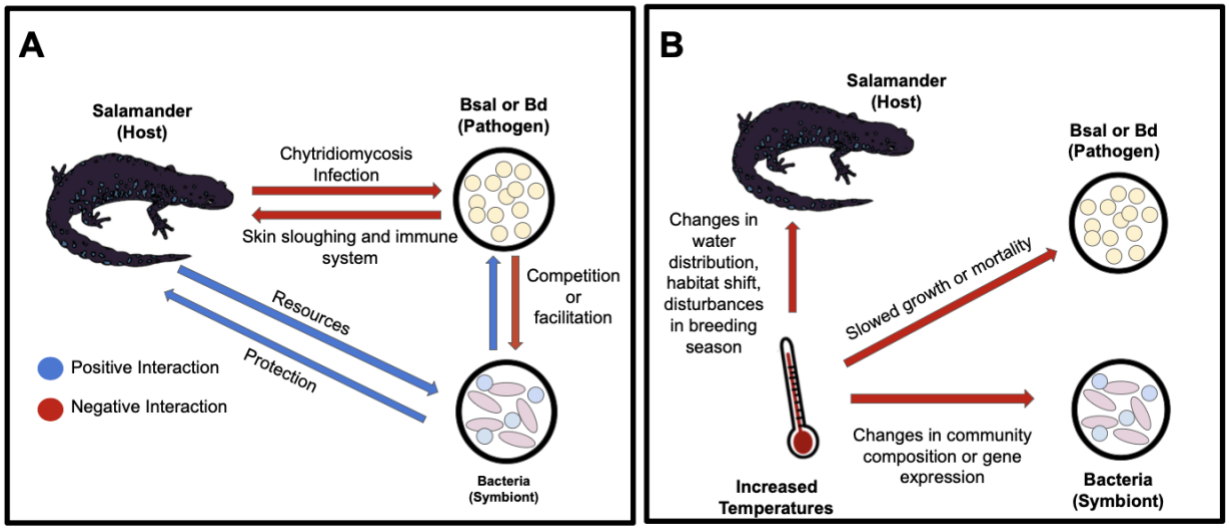

663

Figure 2

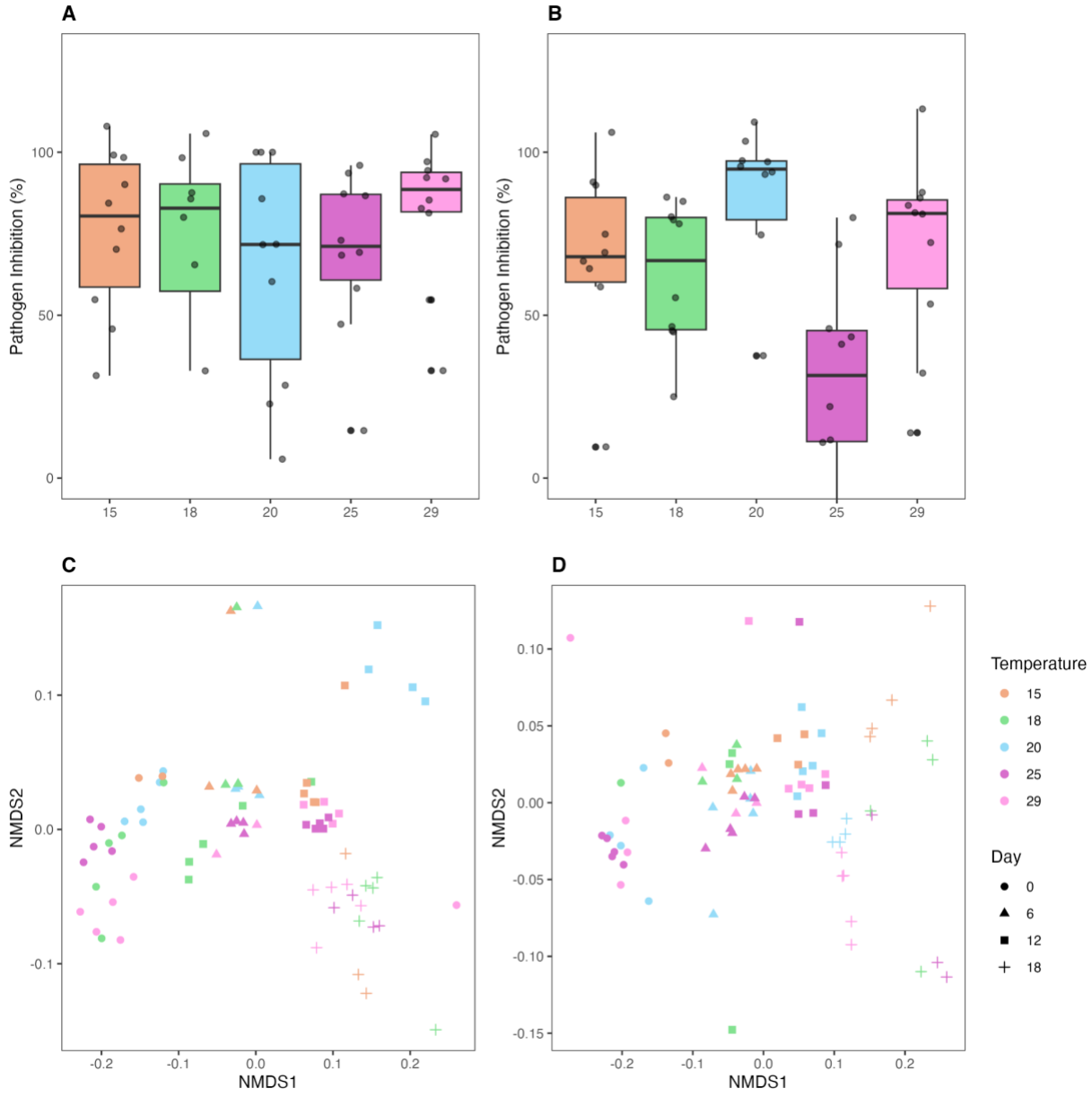
A
B
C
D
Pathogen Inhibition (%)
100
50
0
15
18
20
25
29
NMDS2
NMDS1
0.1
0.0
-0.1
-0.2
0.2
0.10
0.05
0.00
-0.05
-0.10
-0.15
Temperature
15
18
20
25
29
Day
0
6
12
18

Figure 3

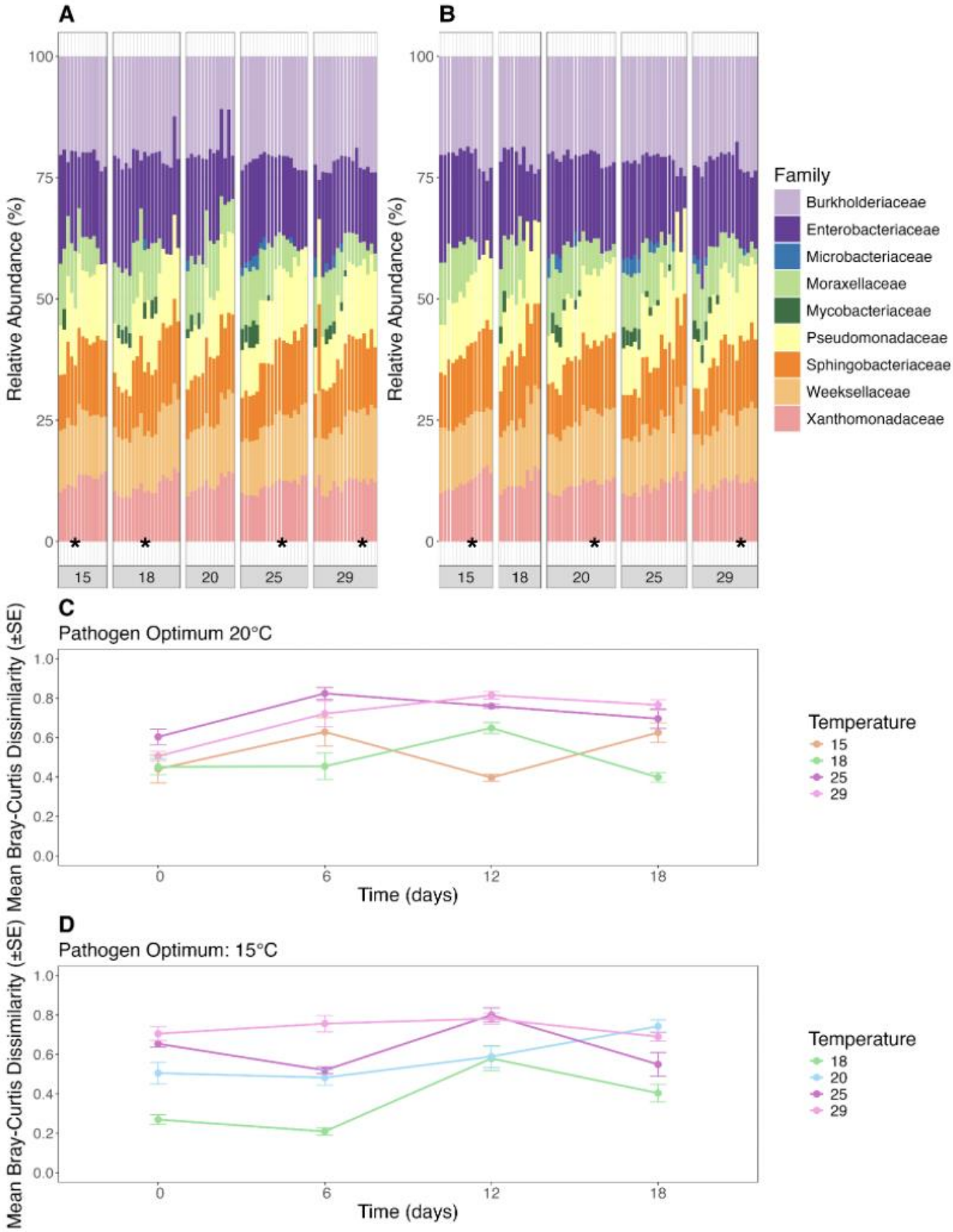
A
B
Relative Abundance (%)
100
75
50
25
0
15
18
20
25
29
Family
Burkholderiaceae
Enterobacteriaceae
Microbacteriaceae
Moraxellaceae
Mycobacteriaceae
Pseudomonadaceae
Sphingobacteriaceae
Weeksellaceae
Xanthomonadaceae
C
Pathogen Optimum 20°C
D
Pathogen Optimum: 15°C
Mean Bray-Curtis Dissimilarity (±SE)
1.0
0.8
0.6
0.4
0.2
0.0
0
6
12
18
Time (days)
Temperature
15
18
20
25
29

668 **Figure 4**

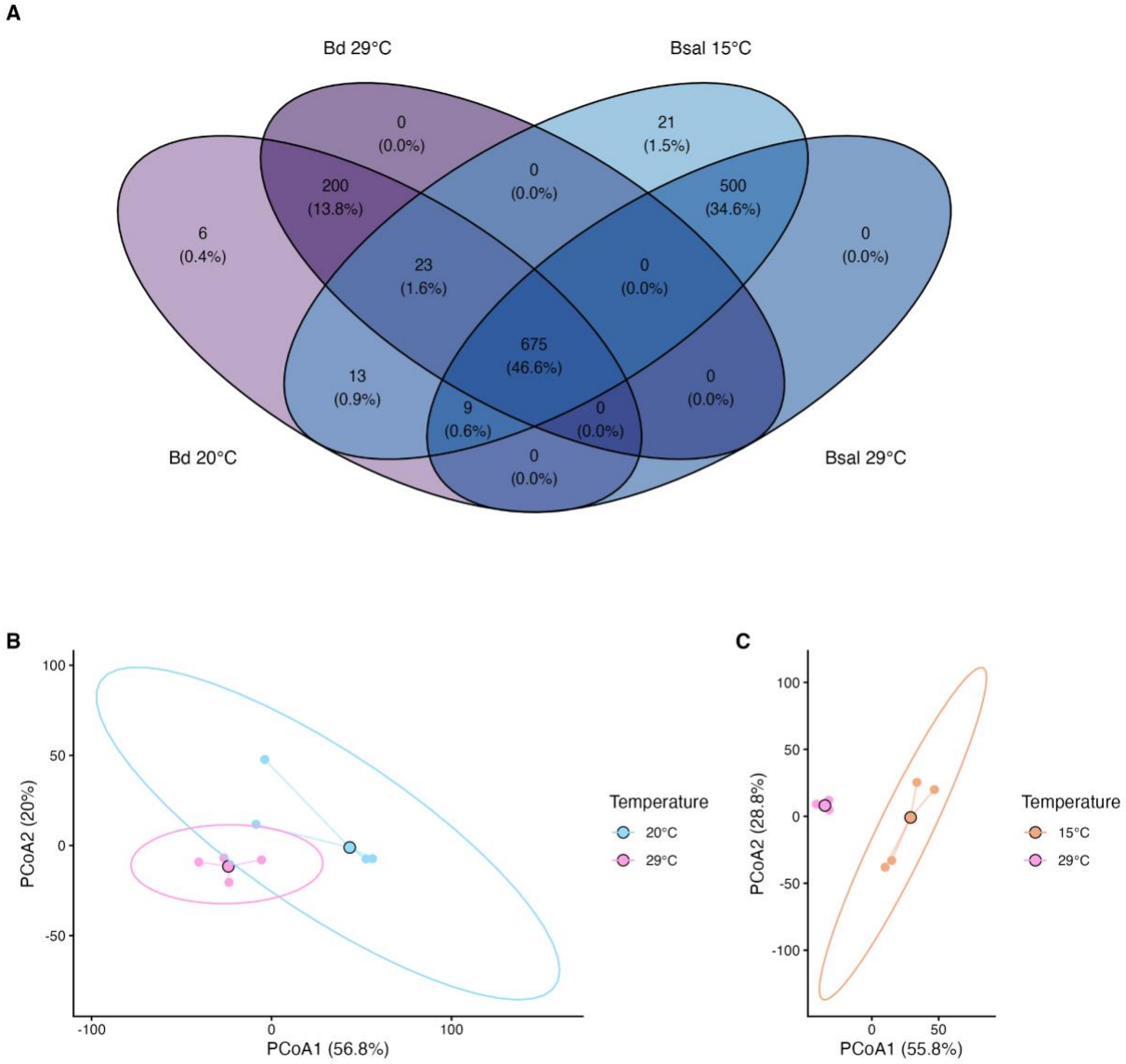

669

Figure 5

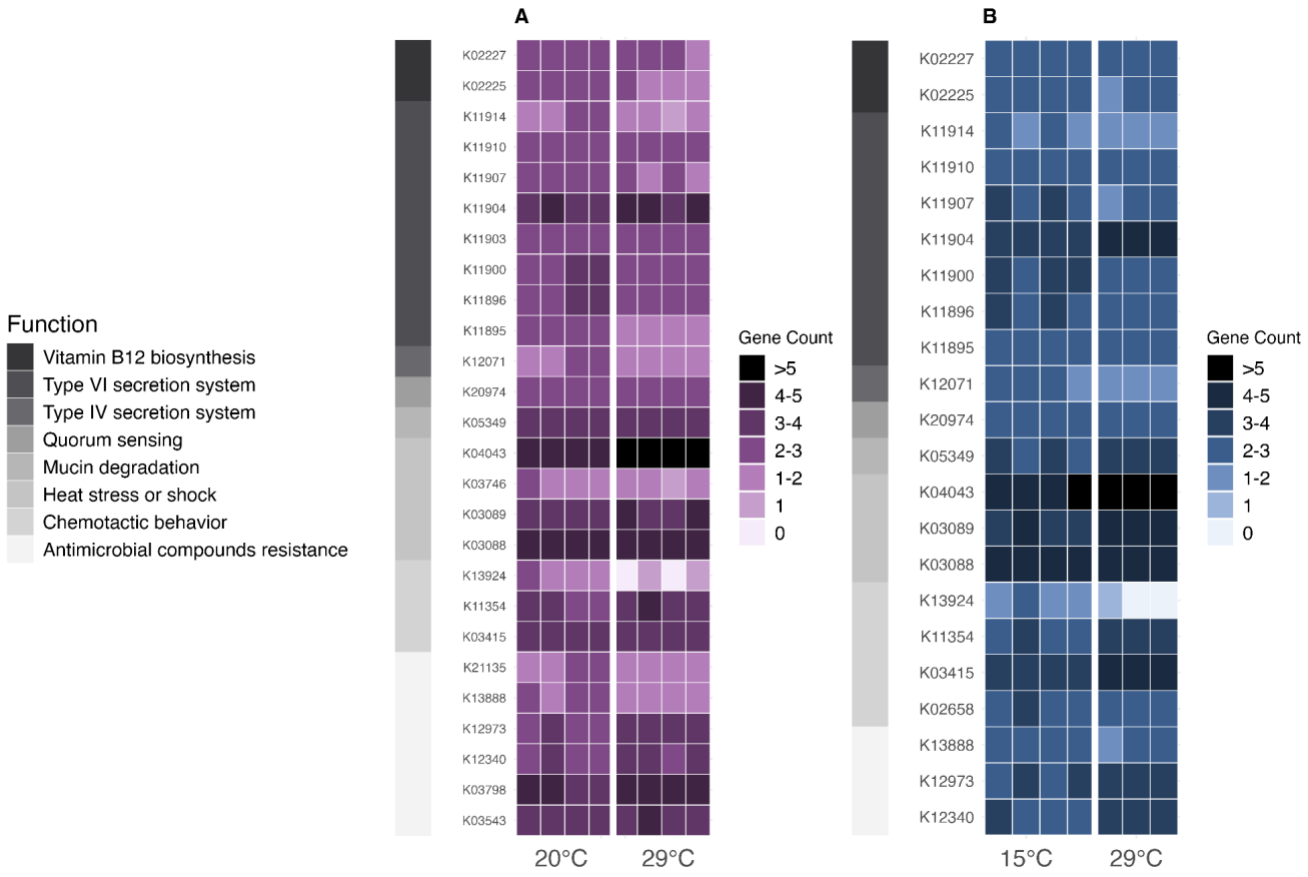
A
B
Function
Vitamin B12 biosynthesis
Type VI secretion system
Type IV secretion system
Quorum sensing
Mucin degradation
Heat stress or shock
Chemotactic behavior
Antimicrobial compounds resistance
K02227
K02225
K11914
K11910
K11907
K11904
K11903
K11900
K11896
K11895
K12071
K20974
K05349
K04043
K03746
K03089
K03088
K13924
K11354
K03415
K21135
K13888
K12973
K12340
K03798
K03543
K02658
Gene Count
>5
4-5
3-4
2-3
1-2
1
0
20°C
29°C
15°C
29°C

Supplemental Materials

Manuscript: *Temperature drives transcriptomic shifts in amphibian skin bacterial communities with consequences for fungal pathogen control*

Authors: Emma G. Thompson & Elle M. Barnes

Table 1. Inhibitory potential of bacterial isolates. Inhibitory potential of bacteria used in SynComs against the fungal pathogen *Batrachochytrium dendrobatidis* (Bd). Identity confirmed via full-length 16S rRNA and whole-genome sequencing (data unpublished).

Species (Isolate ID)	**Inhibitory Potential**	**Genome size (Mb)**
Achromobacter denitrificans (S001B)	Inhibitory	5.4
Acinetobacter calcoaceticus (S001D)	Inhibitory	3.9
Buttiauxella sp. 3AFRM03 (S007B)	Facilitory	5.2
Chryseobacterium indologenes (S005B)	Inhibitory	5.4
Citrobacter braakii (S007A)	Neutral	4.9
Janthinobacterium lividum (912M)	Inhibitory	6.3
Microbacterium oxydans (S005A)	Inhibitory	5.4
Pseudomonas protegens (S007C)	Facilitory	4.5
Serritia fonticola (S002D)	Inhibitory	6.5
Stenotrophomonas humi (S001C)	Neutral	4.1

Table 2. Statistical results for two-way ANOVA on alpha diversity. Comparisons of alpha diversity metrics across five temperatures and four timepoints (day) for SynComs containing Bd or Bsal as the pathogen. Temperature/Day represents the interaction term; $p < 0.05$ is in bold.

Pathogen	Metric	Term	Df	Sum Sq	Mean Sq	F value	Pr(>F)
Bd	*Shannon*	*Temperature*	4	0.2	0.05	1.9	0.12
		Day	1	0.97	0.97	36.19	**4.37E-08**
		Temperature/Day	4	0.28	0.07	2.63	**0.04**
		Residuals	85	2.29	0.03		
	Chao1	*Temperature*	4	13.18	3.3	1.76	0.15
		Day	1	12.21	12.2	6.51	**0.01**
		Temperature/Day	4	5.31	1.33	0.71	0.59
		Residuals	85	159.45	1.88		
	Eveness	*Temperature*	4	0.05	0.01	3.07	**0.02**
		Day	1	0.11	0.11	28.25	**8.47E-07**
		Temperature/Day	4	0.04	0.01	2.51	**0.047**
		Residuals	85	0.32	0.003		
Bsal	*Shannon*	*Temperature*	4	0.17	0.04	1.32	0.27
		Day	1	1.86	0.62	19.55	**1.83E-9**
		Temperature/Day	4	0.71	0.06	1.86	0.053
		Residuals	75	2.39	0.03		
	Chao1	*Temperature*	4	4.88	1.22	0.06	0.69
		Day	1	31.14	31.14	14.56	**0.0002**
		Temperature/Day	4	15.03	3.76	1.76	0.15
		Residuals	85	181.83	2.14		
	Eveness	*Temperature*	4	0.03	0.01	0.09	0.19
		Day	1	0.12	0.12	34.42	**8.31x10-8**
		Temperature/Day	4	0.01	0.002	0.63	0.64

		Residuals	85	0.3	0.004		

Table 3. Results of post hoc testing of alpha diversity by day for SynComs containing Bsal. Post hoc analysis was run on the term Day using the Tukey HSD test since two-way ANOVA revealed $p < 0.05$ for all alpha diversity metrics. Comparisons where *padj* < 0.05 are shown in bold.

Metric	Day	diff	lwr	upr	p adj
Shannon	*6-0*	-0.1260772	-0.2614661	0.009311742	0.0770665
	12-0	-0.2523684	-0.3877573	-0.116979489	**0.0000318**
	18-0	-0.370244	-0.5041558	-0.236332237	**0**
	12-6	-0.1262912	-0.264472	0.011889488	0.0855152
	18-6	-0.2441669	-0.3809006	-0.107433097	**0.0000693**
	18-12	-0.1178756	-0.2546094	0.018858134	0.1155602
Chao1	*6-0*	-0.3170871	-1.396495	0.76232042	0.8668942
	12-0	-0.5607269	-1.640134	0.51868063	0.5250838
	18-0	-1.6058204	-2.673451	-0.53818949	**0.0009805**
	12-6	-0.2436398	-1.345305	0.85802588	0.9374685
	18-6	-1.2887333	-2.378863	-0.19860375	**0.0139381**
	18-12	-1.0450936	-2.135223	0.04503604	0.0650632
Eveness	*6-0*	-0.029287481	-0.07259363	0.01401867	0.2924132
	12-0	-0.084374509	-0.12768066	-0.04106836	**0.0000135**
	18-0	-0.087248492	-0.13008216	-0.04441482	**0.0000054**
	12-6	-0.055087028	-0.09928618	-0.01088788	**0.0085268**
	18-6	-0.057961012	-0.10169733	-0.01422469	**0.0045349**
	18-12	-0.002873983	-0.0466103	0.04086234	0.9981543

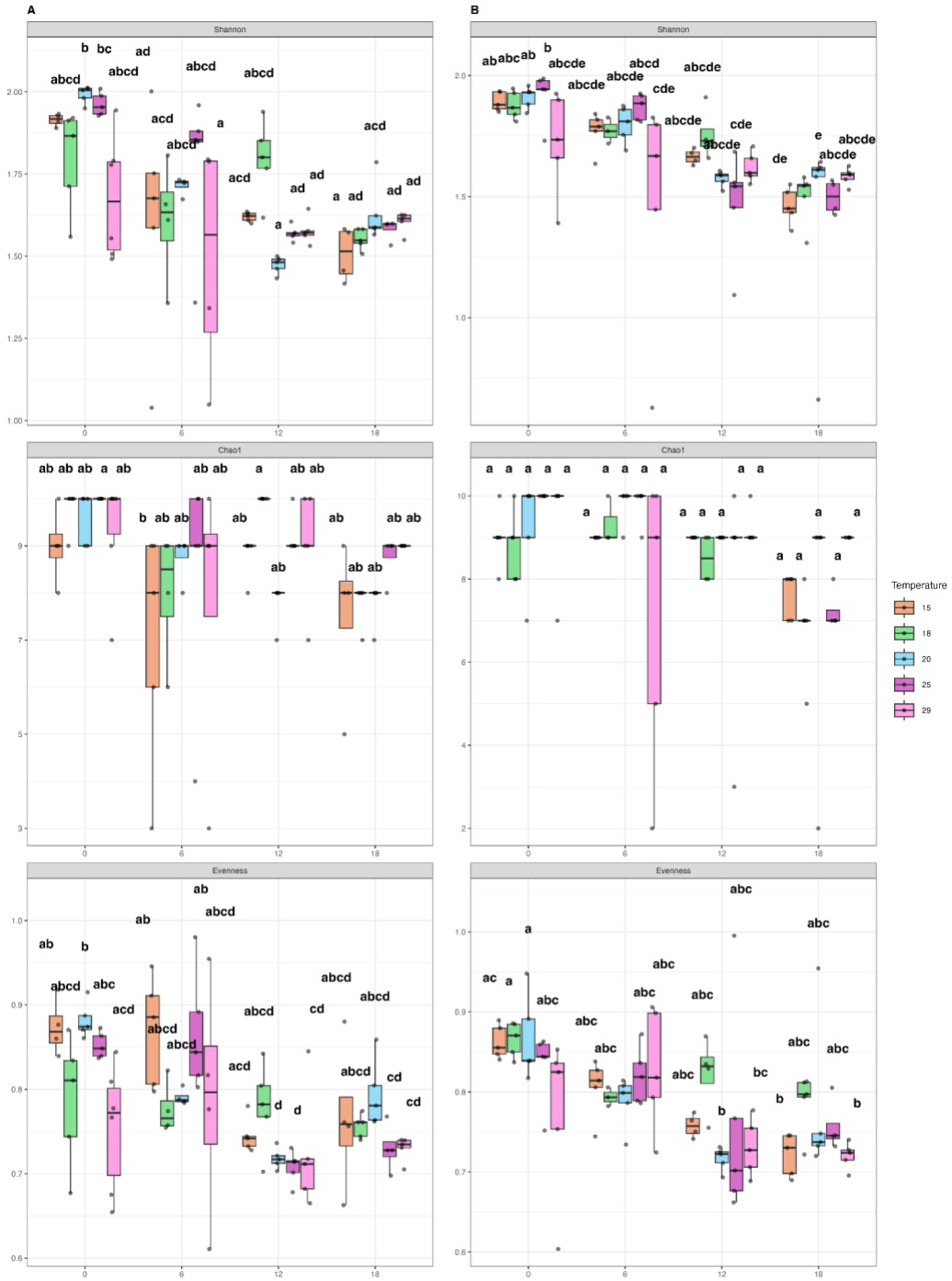

Figure 1. Comparisons of alpha diversity between temperature treatments over time. Alpha diversity in SynComs containing Bd (**A)** or Bsal (**B)** is shown for all metrics: Shannon diversity, Chao1, and evenness indices. Day is on the x-axis and boxplot color corresponds to the trial temperature. Boxplots depict the median and interquartile range (IQR) with whiskers extending to 1.5X IQR, with outliers denoted as solid black points and all points as gray points. Letters represent significant interactions between temperature and day as determined by Tukey post hoc test.

Table 4. Statistical results for PERMANOVA on Community Composition. Comparisons of community composition (measured by Bray-Curtis dissimilarities) across five temperatures and four timepoints (day) for SynComs containing Bd or Bsal as the pathogen. Temperature/Day represents the interaction term; $p < 0.05$ is in bold.

Pathogen	Term	Df	Sum Sq	R^2	F value	Pr(>F)
Bd	*Day*	3	0.32	0.63	58.8	**0.001**
	Temperature	4	8712	2178	2.2	**0.106**
	Temperature/Day	11	0.05	0.09	2.35	**0.006**
	Residuals	20	19801	990.1		
	Total	78	0.51	1		
Bsal	*Day*	3	0.42	0.69	79.35	**0.001**
	Temperature	4	0.03	0.05	4.3	**0.02**
	Temperature/Day	12	0.61	0.1	2.89	**0.001**
	Residuals	57	0.1	0.16		
	Total	76	0.06	1		

Table 5. Comparisons of betadispersion. Samples analyzed for the effects of time (Day) and temperature on dispersion of bacterial communities for SynComs containing either Bd or Bsal.

Pathogen	Term		Df	Sum of Sqs	R^2	F	Pr (>F)
Bd	*Day*	Groups	3	0.005	0.002	1.38	0.26
		Residuals	75	0.08	0.001		
	Temperature	Groups	4	0.006	0.001	0.91	0.46
		Residuals	74	0.14	0.002		
Bsal	*Day*	Groups	3	0.005	0.002	1.38	0.26
		Residuals	75	0.08	0.001		
	Temperature	Groups	4	0.007	0.002	0.91	0.46
		Residuals	74	0.14	0.002		

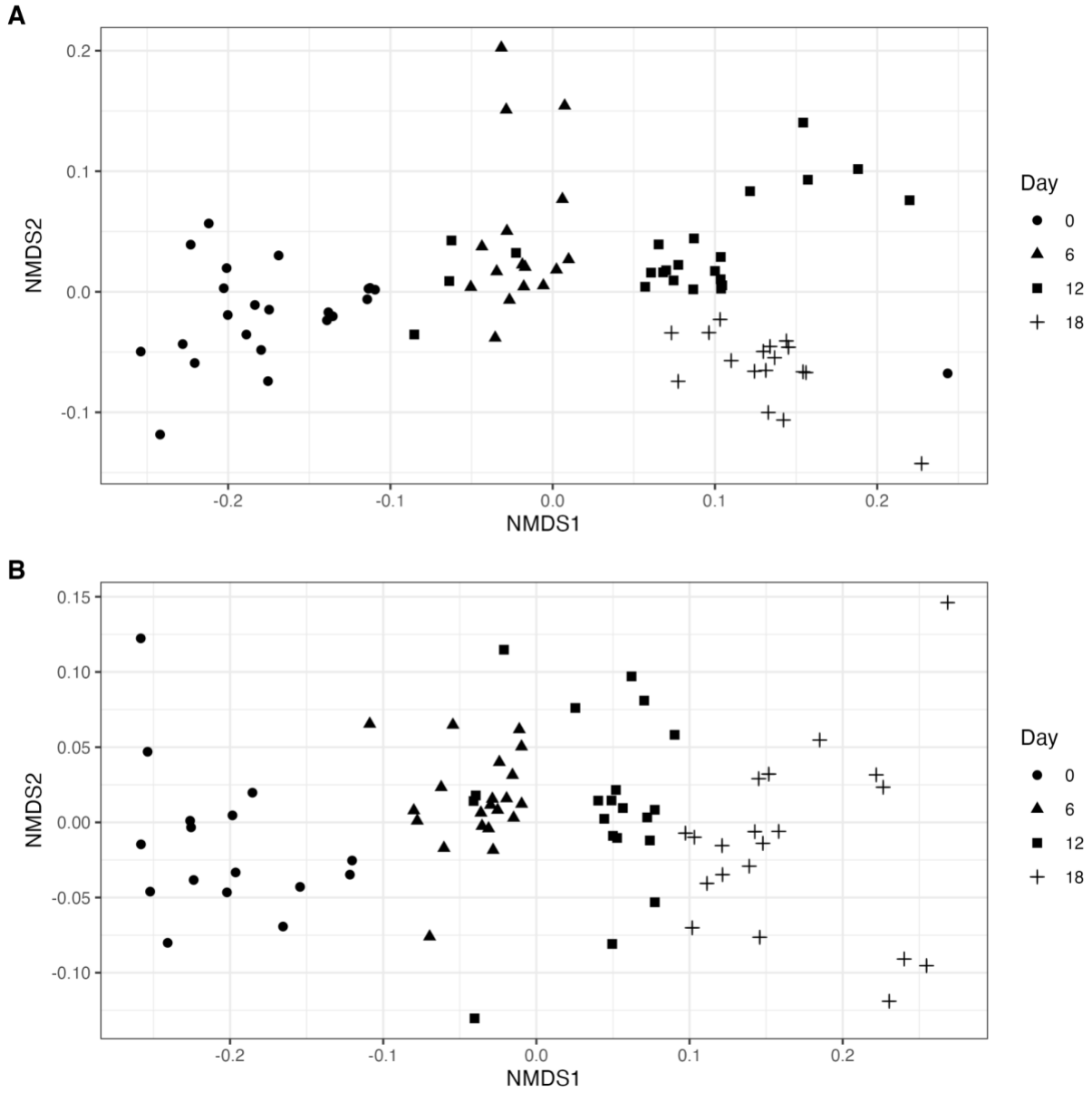

Figure 2. Bacterial community composition over time. Effect of time on composition in SynComs containing Bd (**A**) or Bsal (**B**) was determined via PERMANOVA on weighted UniFrac distances. Shape depicts sampling timepoint. Time had a significant effect on composition: Bd: $F_{(3,20)} = 58.80$, $R^2 = 0.63$, $p = 0.001$; Bsal: $F_{(3,57)} = 79.35$, $R^2 = 0.69$, $p = 0.001$.

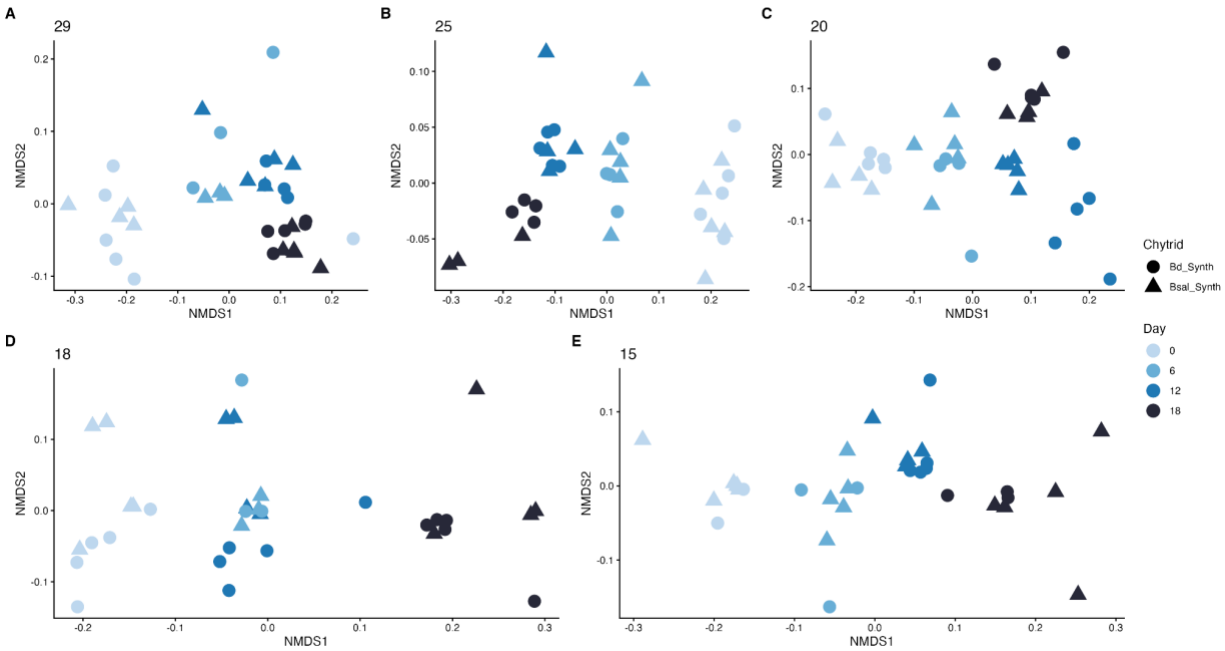

Figure 3. Bacterial community composition over time subset by temperature. Points represent composition in individual SynComs containing Bd or Bsal (represented by shape) over the 18-day experimental period (Day represented by color). Temperature treatments: (**A)** 29°C, (**B)** 25°C, (**C)** 20°C, (**D)** 18°C, and (**E)** 15°C. Data from this figure represent the same data from Figure 2C-D.

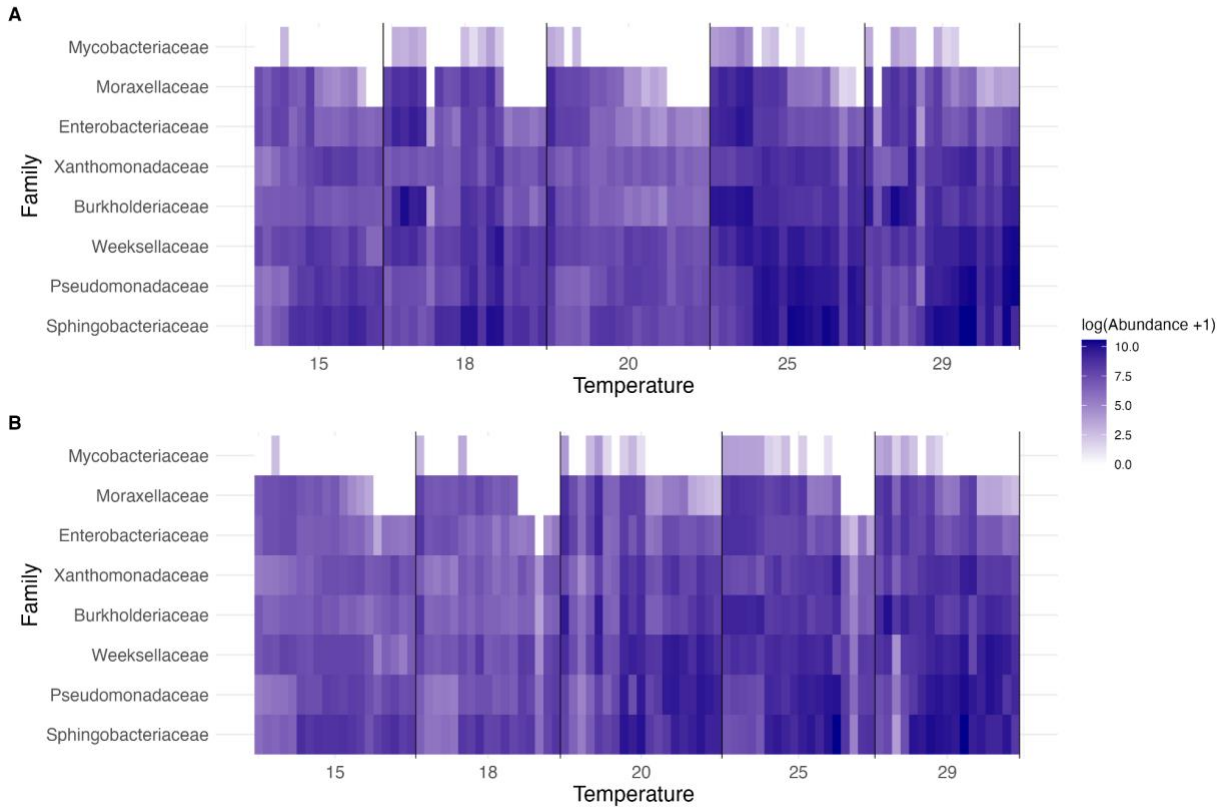

Figure 4. Log abundances of bacterial families over time and across temperature treatments. Samples are ordered by time within each temperature subset. **A** SynComs containing Bd, **B** SynComs containing Bsal.

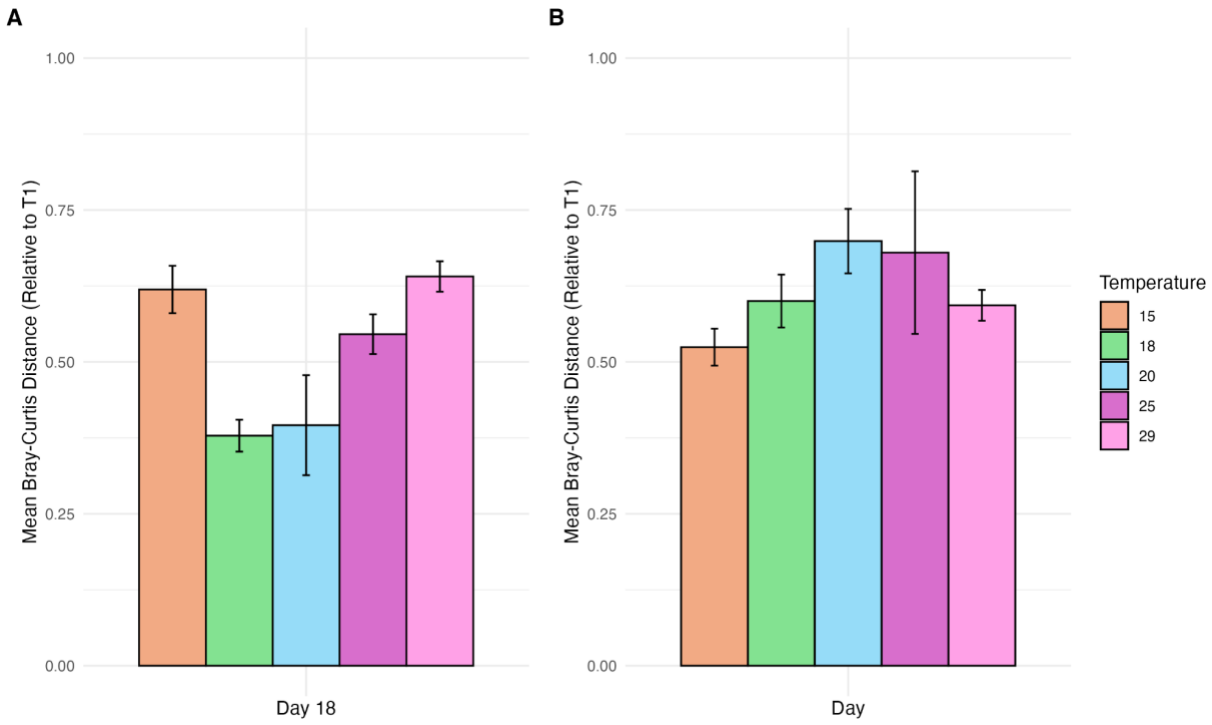

Figure 5. Mean dissimilarity in SynComs at Day 18 compared to Day 0. Dissimilarity was calculated as the mean Bray-Curtis distance between individual Day 18 and Day 0 SynComs within each temperature treatment. SynComs containing Bd (**A)** or Bsal (**B)**.

Table 6. Statistical results for ANOVA on pathogen inhibition. Comparisons of pathogen inhibition across five temperatures for SynComs containing Bd or Bsal; $p < 0.05$ is in bold.

Pathogen	Term	Df	Sum Sq	R^2	F value	Pr(>F)
Bd	*Temperature*	4	8712	0.31	2.2	0.106
	Residuals	20	19801	0.69		
Bsal	*Temperature*	4	18434	0.47	4.469	**0.00963**
	Residuals	20	20622	0.53		

Table 7. Results of post hoc testing of Bsal inhibition by temperature. Post hoc analysis was run on the term Temperature for only SynComs containing Bsal (ANOVA: $p < 0.05$) using the Tukey HSD test. Comparisons where *padj* < 0.05 are shown in bold.

	diff	**lwr**	**upr**	**p adj**
18°C-15°C	24.21	-36.56	84.99	0.76
20°C-15°C	23.62	-37.14	84.4	0.77
25°C-15°C	-50.33	-111.1	10.44	0.14
29°C-15°C	-4.24	-65.02	56.53	0.99
20°C-18°C	-0.59	-61.36	60.18	0.99
25°C-18°C	-74.55	-135.32	-13.77	**0.01**
29°C-18°C	-28.46	-89.23	32.31	0.63
25°C-20°C	-73.96	-134.739	-13.19	**0.01**
29°C-20°C	-27.87	-88.64	32.9	0.65
29°C-25°C	46.09	-14.68	106.86	0.2

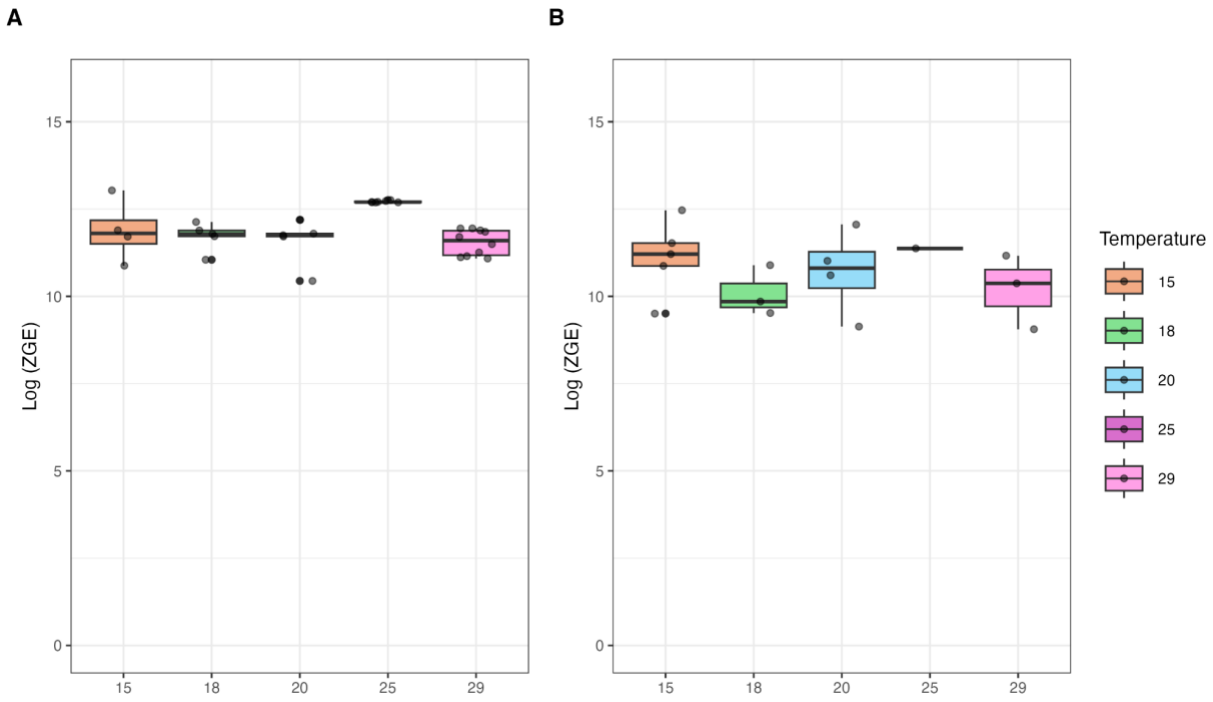

Figure 6. Pathogen abundance on day 18 for each experimental temperature. Log abundance of zoospore genomic equivalents (ZGEs) of Bd (**A**) and Bsal (**B**) on day 18 measured by qPCR. Boxplots shows median and interquartile range with whiskers extending to 1.5X interquartile range, with outliers denoted as solid black points and all points as gray points. Log abundance was analyzed via one-way ANOVA ; Bd: $F_{(1,30)} = 0.001$, $p = 0.97$; Bsal: $F_{(1,20)} = 3.4$, $p = 0.08$.

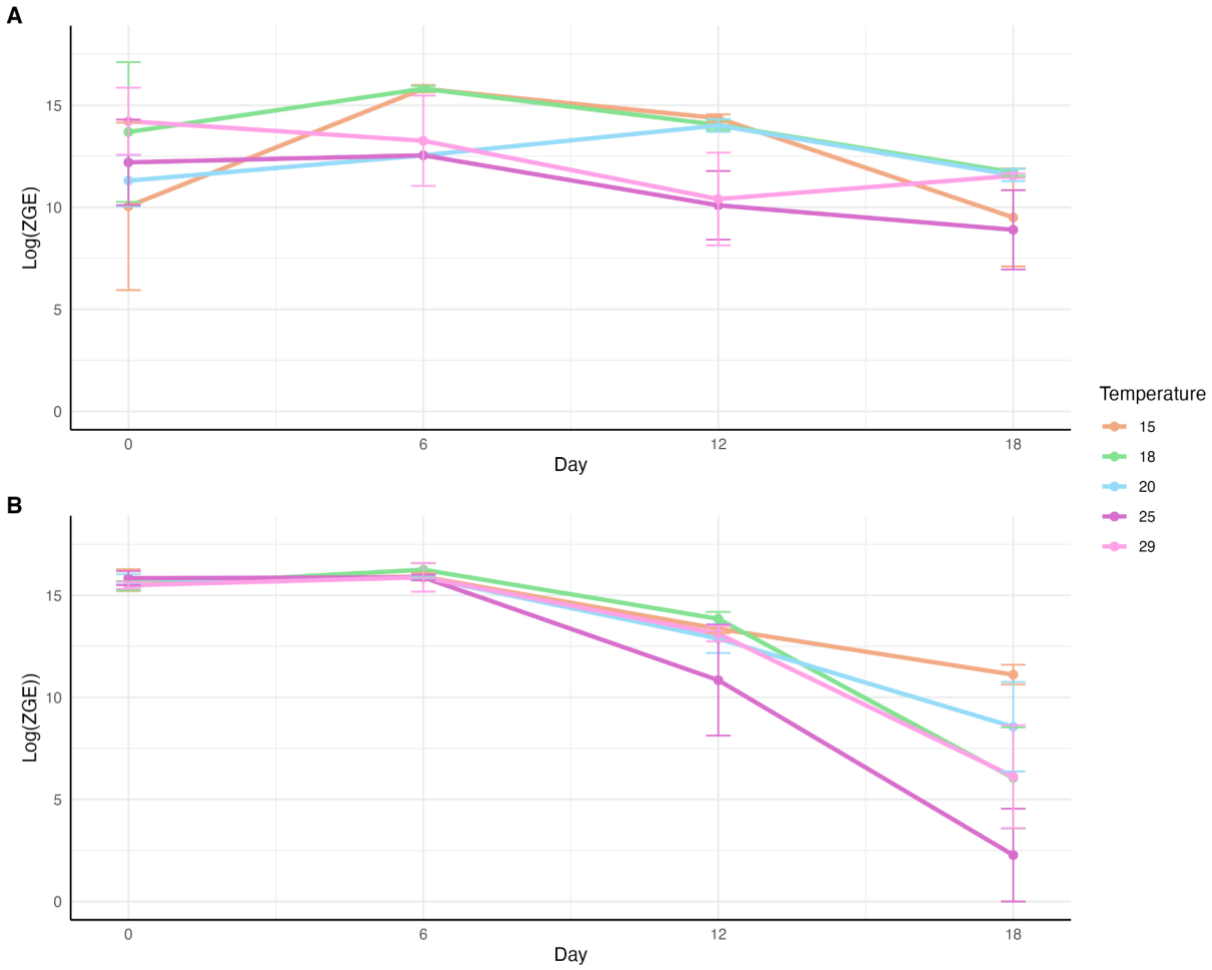

Figure 7. Pathogen abundance over time for each experimental temperature. Mean log zoospore genomic equivalent (ZGEs) and standard error for Bd (**A**) or Bsal (**B**) were measured every six days (n = 5) via qPCR. For reference: Bd's thermal optimum is 20°C, and Bsal's is 15°C.

Table 8. Statistical results for two-way ANOVA on pathogen abundance. Comparisons of zoospore genomic equivalents (ZGEs; measured by qPCR and log-transformed) across five temperatures and four timepoints (day) for SynComs containing Bd or Bsal as the pathogen. Temperature/Day represents the interaction term; $p < 0.05$ is in bold.

Pathogen	Term	Df	Sum Sq	Mean Sq	F value	Pr (>F)
Bd	*Temperature*	4	1.09E+15	2.74E+14	9.7	**6.73e-07**
	Day	3	2.06E+15	6.88E+14	24.4	**1.37e-12**
	Temperature/Day	12	1.62E+15	1.35E+14	4.78	**1.89e-06**
	Residuals	130	3.66E+15	2.82E+13		
Bsal	*Temperature*	4	2.88E+14	7.20E+13	0.41	0.8
	Day	3	3.10E+15	1.03E+15	5.91	**0.0011**
	Temperature/Day	12	1.48E+15	1.23E+14	0.7	0.74
	Residuals	80	1.40E+16	1.75E+14		

Table 9. Results of post hoc testing of Bsal abundance by day. Post hoc analysis was run on the term Day for only SynComs containing Bsal using the Tukey HSD test as this was the only significant term in the two-way ANOVA. Comparisons where *padj* < 0.05 are shown in bold.

	diff	**lwr**	**upr**	**p adj**
6-0	5740994.7	-4080966	15562956	0.42
12-0	-7106698.5	-16928660	2715262	0.24
18-0	-7875590.2	-17697551	1946371	0.16
12-6	-12847693.2	-22669654	-3025732	**0.005**
18-6	-13616584.9	-2343854	-3794624	**0.003**
18-12	-768891.6	-10590853	9053069	0.99

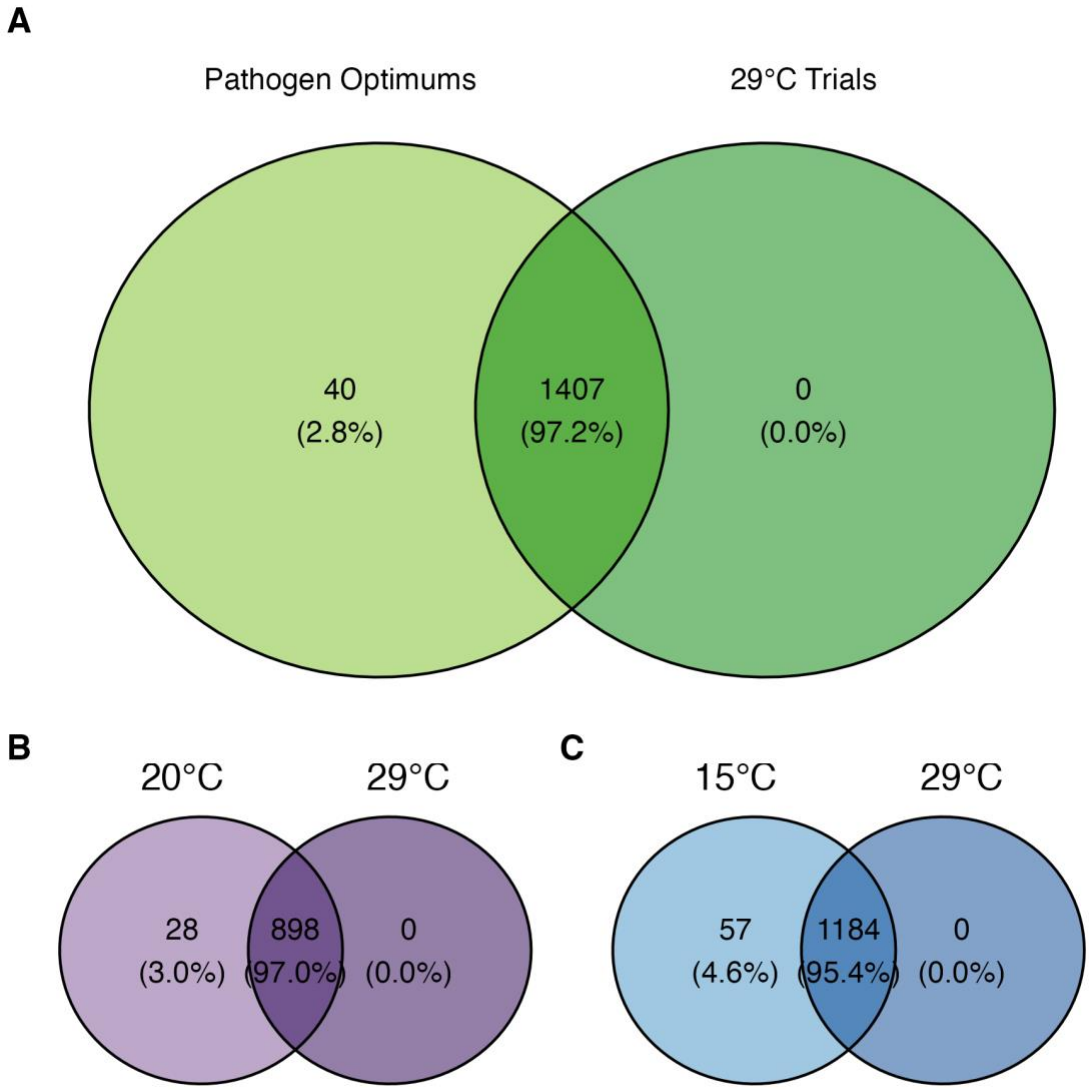

Figure 8. Venn diagrams comparing differentially expressed genes between treatments. Differentially expressed genes between 15°C and 29°C at $p_{adj} < 0.05$ and logFC > 1 were compared between trials. Genes expressed within each experimental group and shared between groups represent a percentage of the total number of genes expressed during the trial.

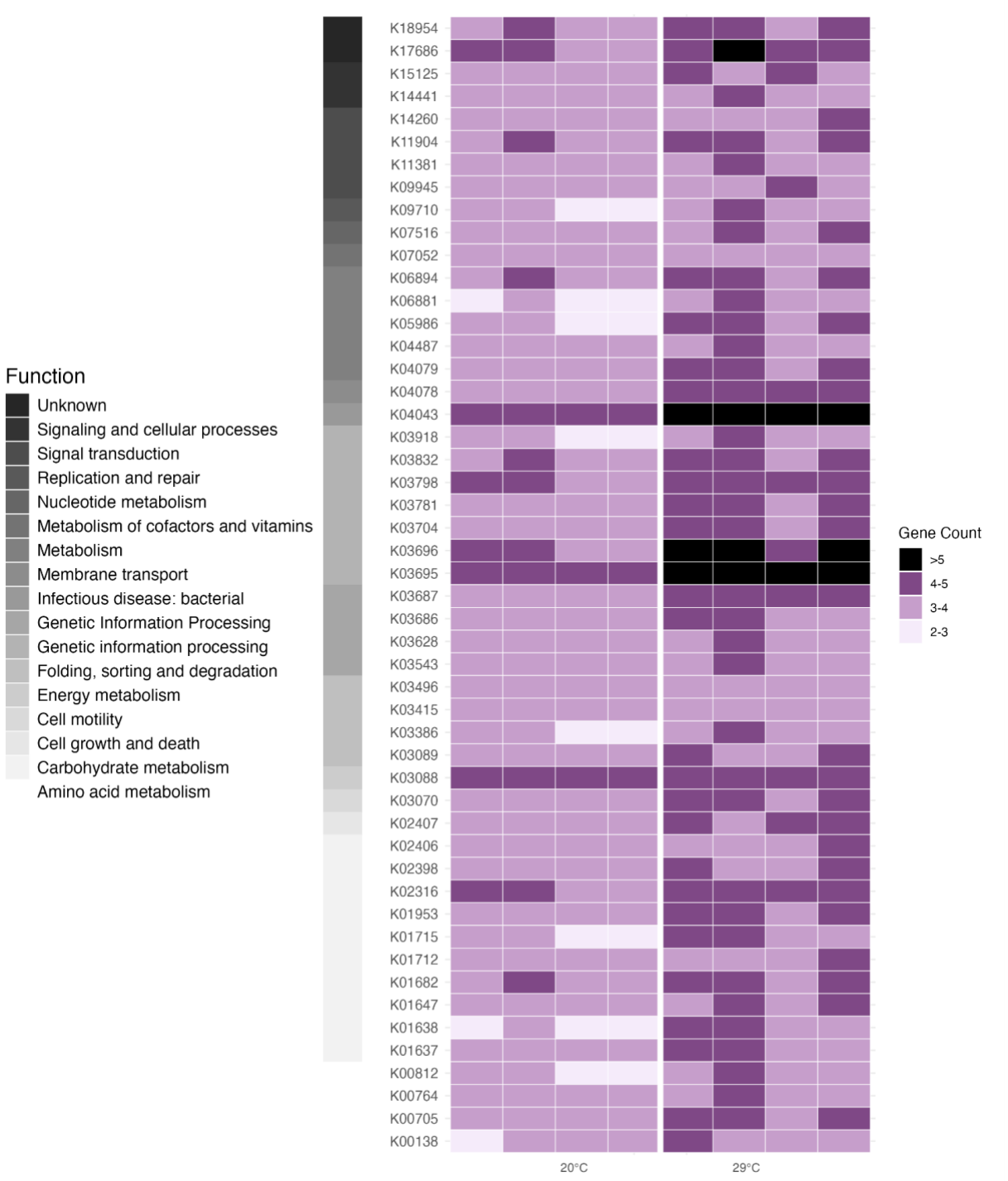

Figure 9. Comparison of differentially expressed genes in the Bd microcosms at 20 vs. 29°C. Heat map of the top 50 differentially expressed KOs (i.e., $p_{adj} < 0.05$ and logFC > 1) between the 20°C (thermal optimum) and 29°C treatments ordered by their KEGG Orthology identifier. Columns represent metatranscriptomic replicates, heatmap color denotes DESeq2-normalized gene counts, and gray scale identifies the functional group of each KO.

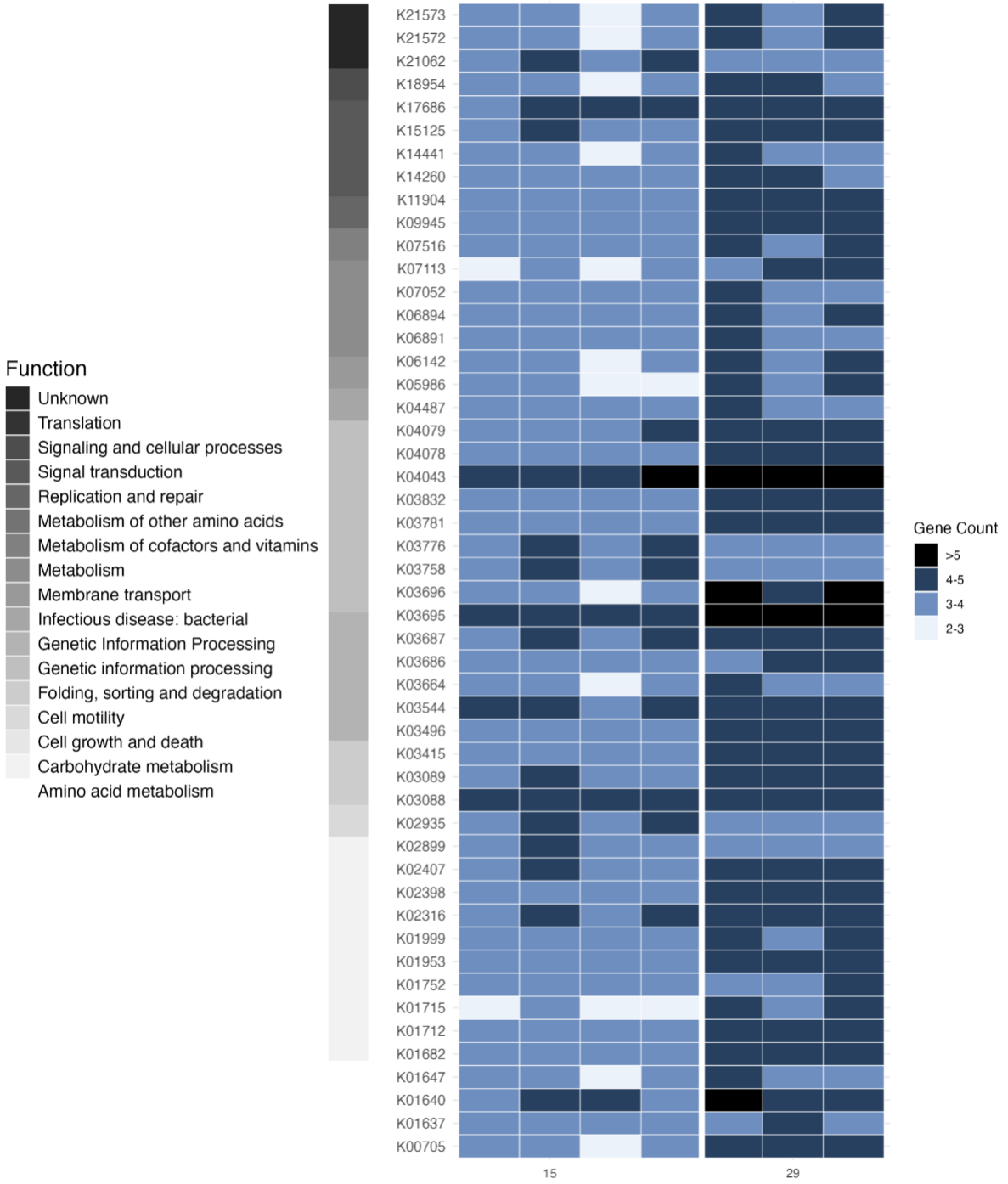

Figure 10. Comparison of differentially expressed genes in the Bsal microcosms at 15 vs. 29°C. Heat map of the top 50 differentially expressed genes (i.e., $p_{adj} < 0.05$ and logFC > 1) between the 15°C (thermal optimum) and 29°C treatments ordered by their KEGG Orthology identifier. Columns represent metatranscriptome replicates, heatmap color denotes DESeq2-normalized gene counts, and gray scale identifies the functional group of each KO.

Table 10. Statistical results for PERMANOVA on Gene Expression. Gene expression across thermal optimum (15°C Bsal & 20°C Bd) temperatures and highest trial temperature (29°C) for SynComs containing Bd or Bsal as the pathogen.

Pathogen	Term	Df	Sum of Sqs	R2	F	Pr(>F)
Bd	*Temperature*	1	5772.6	0.37	3.49	**0.04**
	Residual	6	9925	0.63		
	Total	7	15697.6	1		
Bsal	*Temperature*	1	6888.1	0.52	5.37	**0.04**
	Residual	5	6413.6	0.48		
	Total	6	13301.7	1		